AD-A046 714 BOLT BERANEK AND NEWMAN INC ARLINGTON VA F/G 20/1
STATISTICAL MEASURES OF AMBIENT NOISE: ALGORITHMS, PROGRAM, AND--ETC(U)
JUN 77 M MOLL, R M ZESKIND, F J SULLIVAN N00014-71-C-0303
UNCLASSIFIED BBN-3390 NL

1 OF 2
AD A046714

(12)

Report No. 3390

STATISTICAL MEASURES OF AMBIENT NOISE: ALGORITHMS, PROGRAM, AND PREDICTIONS (U)

M. Moll
R. M. Zeskind
P. J. M. Sullivan

June 1977

Contract No. N00014-71-C-0303
Task No. NR 274-236
BBN Job No. 10295

Submitted to:

Naval Analysis Program
Office of Naval Research
Department of the Navy
800 North Quincy Street
Arlington, VA 22217

Attention: Mr. James G. Smith
Code 431

Naval Electronic Systems Command
Department of the Navy
Washington, D.C. 20360

Attention: Code 320

Submitted by:

Bolt Beranek and Newman Inc.
1701 North Fort Myer Drive
Arlington, VA 22209

Reproduction in whole or in part is permitted for any purpose of the United States Government.

Approved for Public Release; Distribution Unlimited.

Unclassified

SECURITY CLASSIFICATION OF THIS PAGE (When Data Entered)

REPORT DOCUMENTATION PAGE		READ INSTRUCTIONS BEFORE COMPLETING FORM
1. REPORT NUMBER: 3390	2. GOVT ACCESSION NO.	3. RECIPIENT'S CATALOG NUMBER
4. TITLE (and Subtitle): (6) Statistical Measures of Ambient Noise: Algorithms, Program, and Predictions.		5. TYPE OF REPORT & PERIOD COVERED: (9) Technical rept.,
		6. PERFORMING ORG. REPORT NUMBER: (14) BBN [redacted]3390
7. AUTHOR(S): (10) M./Moll, R. M./Zeskind, F. J. M./Sullivan		8. CONTRACT OR GRANT NUMBER(S): (15) N00014-71-C-0303
9. PERFORMING ORGANIZATION NAME AND ADDRESS: Bolt Beranek and Newman Inc. 1701 North Fort Myer Drive Arlington, VA. 22209		10. PROGRAM ELEMENT PROJECT TASK AREA & WORK UNIT NUMBERS: 65152N NR 274-236 (16) RO145
11. CONTROLLING OFFICE NAME AND ADDRESS: Naval Analysis Programs (Code 431) Office of Naval Research Arlington, VA. 22217		12. REPORT DATE: (11) Jun[redacted]77
		13. NUMBER OF PAGES: ~~97~~ (12) 111
14. MONITORING AGENCY NAME & ADDRESS (if different from Controlling Office)		15. SECURITY CLASS. (of this report): Unclassified
		15a. DECLASSIFICATION/DOWNGRADING SCHEDULE: N/A

16. DISTRIBUTION STATEMENT (of this Report)

Approved for Public Release; Distribution Unlimited.

17. DISTRIBUTION STATEMENT (of the abstract entered in Block 20, if different from Report)

18. SUPPLEMENTARY NOTES

This development was jointly supported by the Office of Naval Research, Code 431, and the Naval Electronic Systems Command, Code 320.

19. KEY WORDS (Continue on reverse side if necessary and identify by block number)

Statistical measures of underwater ambient noise

20. ABSTRACT (Continue on reverse side if necessary and identify by block number)

In a band of rather low frequencies, almost all of the ambient noise in the ocean is generated by ship traffic. If the averaged squared noise pressure in this band is monitored at a point in the ocean, it would be found to fluctuate in a random manner. For a given time, this quantity can be regarded as a random variable X characterized by a probability density function. Although this function contains information about the variability of X, it gives no information about its time varia-→

DD FORM 1 JAN 73 1473 EDITION OF 1 NOV 65 IS OBSOLETE

Unclassified

SECURITY CLASSIFICATION OF THIS PAGE (When Data Entered)

406 454

If X_τ represents observations taking place τ time units after observations X, the joint probability density of X and X_τ contains information about the average time variation of X. From this density, lower-order statistical measures can be derived.

In order to predict surveillance system performance, the directional characteristics of shipping noise must also be considered. For a first level of approximation, this can be done by predicting the noise arriving from ships within narrow azimuth sectors.

The algorithm derived for the calculation of the joint density of X and X_τ is organized according to shipping routes in an acoustic basin, and the types of ships on those routes. The algorithm first calculates the joint characteristic function and then transforms it to obtain the joint density function.

One of the inputs required by the algorithm is a set of source characteristic functions, one for each type of ship represented for each frequency band of interest. A means has been devised for calculating these characteristic functions from the predicted characteristics of noise-generating mechanisms aboard the ships.

Currently, the program is implemented to calculate the first-order density of X, and to utilize that density for the calculation of mean and variance. Also available is the density of $10 \log_{10} X$, from which the distribution function can be obtained.

Three sets of examples have been run to demonstrate and check the program. The parameters that were varied include the average number of ships per mile of route, the range to the intersection of the nominal route and the center of the observation sector, and the width of the route. The results agree with those obtained by alternative calculations based on Campbell's Theorem.

ACCESSION for
NTIS White Section
DDC Buff Section
UNANNOUNCED
JUSTIFICATION
BY
DISTRIBUTION/AVAILABILITY CODES
Dist. SPECIAL
A

Table of Contents

		Page
Report Documentation Page		ii
Table of Contents		iv
List of Tables		vi
List of Figures		vii
Summary		x
1.0	INTRODUCTION	1
1.1	Background	1
1.2	Averaged Squared Pressure	5
1.3	Approach	7
2.0	THE JOINT CHARACTERISTIC FUNCTION	15
2.1	Derivation	15
2.2	Relationship of Coordinates	19
3.0	FOURIER TRANSFORM ALGORITHMS FOR LOGARITHMICALLY SAMPLED DATA	23
3.1	Fourier Transform Algorithm	24
3.2	Inverse Fourier Transform	34
3.3	Two-Dimensional Inverse Fourier Transform	38
4.0	CHARACTERISTIC FUNCTIONS FOR SOURCES	47
4.1	Introduction	47

Table of Contents (concluded)

	Page
4.2 Narrowband Sources	49
4.3 Broadband Component	53
4.4 Results of Calculations	57
5.0 DESCRIPTION OF COMPUTER PROGRAM	69
6.0 EXAMPLES	72
6.1 Example 1 — Various Ship Traffic Densities	73
6.2 Example 2 — Variation in Range	78
6.3 Example 3 — Variation in the Width of the Route	84
APPENDIX A: RELATIONSHIP OF COORDINATES	87
APPENDIX B: A SHIP TRAFFIC MODEL	94
Distribution List	98

List of Tables

		Page
Table 1.1	Required Statistical Measures.....	4
Table 4.1	Moments of Total Radiated Noise Density for 1-Hz Band at 100 Hz.....	68
Table 6.1	Some Statistical Measures of the Received Noise for Three Ship Traffic Densities.....	77
Table 6.2	Statistical Measures of Received Noise for Two Ranges..	83
Table 6.3	Statistical Measures for Example 3.....	86

List of Figures

		Page
FIGURE 1.1	BASIN CONCEPT.....	10
FIGURE 1.2	INTERSECTION OF A SECTOR WITH A ROUTE ENVELOPE.....	12
FIGURE 2.1	COORDINATE SYSTEM.....	21
FIGURE 3.1	PIECEWISE-LINEAR APPROXIMATION OF PROBABILITY DENSITY FUNCTION.....	26
FIGURE 3.2	PIECEWISE-LINEAR APPROXIMATION FOR THE n^{th} INTERVAL..	28
FIGURE 3.3	ACCURACY OF FOURIER TRANSFORM ALGORITHM; REAL PART OF FOURIER TRANSFORM OF UNIFORM DENSITY FUNCTION.....	32
FIGURE 3.4	ACCURACY OF FOURIER TRANSFORM ALGORITHM; IMAGINARY PART OF FOURIER TRANSFORM OF UNIFORM DENSITY.....	33
FIGURE 3.5	ACCURACY OF INVERSE FOURIER TRANSFORM ALGORITHM.....	39
FIGURE 3.6	SAMPLE POINTS IN α,β PLANE SHOWING A GENERAL SEGMENT.	42
FIGURE 4.1	NARROWBAND PROBABILITY DISTRIBUTION: LARGE MERCHANT VESSELS, DIESEL FIRING RATE.....	50
FIGURE 4.2	BROADBAND ACOUSTIC CLASS SPECTRA.....	54
FIGURE 4.3	DISTRIBUTION OF BROADBAND CLASSES, MERCHANT VESSELS LESS THAN 700 FT. LOA.....	55

List of Figures (cont'd)

		Page
FIGURE 4.4	DISTRIBUTION OF BROADBAND CLASSES, MERCHANT VESSELS GREATER THAN 700 FT. LOA.....	56
FIGURE 4.5	DIESEL FIRING RATE DENSITY FUNCTION FOR MERCHANT SHIPS LESS THAN 700 FT. [FREQ = 100 HZ].....	58
FIGURE 4.6	BLADE RATE DENSITY FUNCTION FOR MERCHANT SHIPS LESS THAN 700 FT. [FREQ = 100 HZ].....	59
FIGURE 4.7	BROADBAND DENSITY FUNCTION FOR MERCHANT SHIPS LESS THAN 700 FT. [FREQ = 100 HZ].....	60
FIGURE 4.8	DIESEL FIRING RATE DENSITY FUNCTION FOR MERCHANT SHIPS GREATER THAN 700 FT. [FREQ = 100 HZ].....	61
FIGURE 4.9	BLADE RATE DENSITY FUNCTION FOR MERCHANT SHIPS GREATER THAN 700 FT. [FREQ = 100 HZ].....	62
FIGURE 4.10	BROADBAND DENSITY FUNCTION FOR MERCHANT SHIPS GREATER THAN 700 FT. [FREQ = 100 HZ].....	63
FIGURE 4.11	BLOCK DIAGRAM OF TOTAL RADIATED NOISE COMPUTER PROGRAM.....	65
FIGURE 4.12	TOTAL RADIATED NOISE PROBABILITY DENSITY FUNCTION OF SOURCE LEVEL FOR MERCHANT SHIPS LESS THAN 700 FT. LOA [FREQ = 100 HZ].....	66
FIGURE 4.13	TOTAL RADIATED NOISE PROBABILITY DENSITY FUNCTION OF SOURCE LEVEL FOR MERCHANT SHIPS GREATER THAN 700 FT. LOA [FREQ = 100 HZ].....	67

List of Figures (concluded)

		Page
FIGURE 5.1	COMPUTER PROGRAM BLOCK DIAGRAM.....	70
FIGURE 6.1	ROUTE AND SENSOR GEOMETRY FOR THE EXAMPLE OF SECTION 6.1.....	74
FIGURE 6.2	PROBABILITY DENSITY FUNCTIONS OF THE RECEIVED NOISE FOR THREE SHIP TRAFFIC DENSITIES: (a) 0.025 ships/n.m. (b) 0.050 ships/n.m. (c) 0.100 ships/n.m.....	75
FIGURE 6.3	PROBABILITY DISTRIBUTION FUNCTIONS OF THE RECEIVED NOISE FOR THREE SHIP TRAFFIC DENSITIES.....	76
FIGURE 6.4	ROUTE AND SENSOR GEOMETRY FOR THE EXAMPLE OF SECTION 6.2.....	79
FIGURE 6.5	PROBABILITY DENSITY FUNCTIONS OF RECEIVED NOISE FOR TWO DIFFERENT RANGES.....	81
FIGURE 6.6	PROBABILITY DISTRIBUTION FUNCTIONS OF RECEIVED NOISE FOR TWO RANGES.....	82
FIGURE 6.7	ROUTE AND SENSOR GEOMETRY FOR EXAMPLE THREE.....	85
FIGURE A.1	FIRST SPHERICAL TRIANGLE.....	88
FIGURE A.2	SECOND SPHERICAL TRIANGLE.....	88
FIGURE B.1	REPRESENTATION OF A TRADE ROUTE.....	95

Summary

As new acoustic surveillance systems are developed by the Navy, answers will be needed to questions such as:

- Where should these systems be deployed?
- How many and what kind are needed for effective surveillance?
- How should new system techniques be utilized?
- Will these systems still be effective in the future when trade routes have changed and new classes of ships ply the waters?

Since the cost of these new systems will be quite high, we would like to be able to predict the answers to those questions before the systems are developed and emplaced.

Answering the questions above requires a performance prediction capability which, in turn, requires an ability to accurately predict crucial characteristics of ambient noise. This report describes an approach to the calculation of the effects of ambient shipping noise on the detection performance of undersea surveillance sensors.

In a band of rather low frequencies, almost all of the ambient noise in the ocean is generated by ship traffic. If the squared noise pressure in the band is monitored at a point

and a short-term (on the order of a minute) running average is obtained, it would be found that the running average fluctuates with time, in an unpredictable manner. It is thus reasonable to consider the averaged squared noise pressure at a point at a given time as a random variable X characterized by a probability density function. Although this function contains information about the variability of X, it gives no information about its time variation.

If X_τ represents observations taking place at τ time units after observations X, the joint probability density of X and X_τ contains information about the average time variation of X. From this joint density, lower-order statistical measures can be derived.

In order to predict surveillance system performance, the directional characteristics of shipping noise must also be considered. For a first level of approximation, this can be done by predicting the noise arriving from ships within narrow sectors of azimuth.

The algorithm derived for the calculation of the joint density of X and X_τ is organized according to shipping routes in an acoustic basin, and the types of ships on those routes. The algorithm first calculates the joint characteristic function and then transforms it to obtain the joint density function.

One of the inputs required by the algorithm is a set of source characteristic functions, one for each type of ship represented for each frequency band of interest. A means has been devised for calculating these characteristic functions from the predicted characteristics of noise generating mechanisms aboard the ships.

The signature components included are (1) the broadband component generated by the collapse of propeller cavitation bubbles; (2) narrowband components at the propeller blade rate and its harmonics; (3) narrowband components at the diesel firing rate and its harmonics; and (4) the narrowband component at the ship's electric plant frequency.

Currently, the program is implemented to calculate the first-order density of X, and to utilize that density for the calculation of mean and variance. That density can also be transformed to obtain the density of $10 \log_{10} X$ from which its distribution function can be obtained.

Three sets of examples have been run to demonstrate and check the program.

In the first set of examples, the average number of ships per route mile (average density) was varied. The calculated means and variances varied in direct proportion to the average density as expected.

In the second set of examples, the range was varied. In this case, the mean value remained nearly constant because the effects of the change of range on the transmission loss were offset by the average number of ships in the observation sector. At the shorter range, the variance was slightly greater because of the increased variability related to the smaller population of ships in the observation sector.

In the third set of examples, the width of the shipping route was varied, Here the principal effect is an increase of variance with route width due to the greater uncertainty in the position of the ships.

In summary, the predictions agreed qualitatively with all expectations, and agreed quantitatively with the alternative calculations produced for the first two sets of examples.

1.0 INTRODUCTION

1.1 Background

As new acoustic surveillance systems are developed by the Navy a continuing set of questions will have to be answered concerning their geographic deployment, the number and mix of the systems, and the effects of changing environmental noise conditions. Since the cost of these systems will be high, we would like to be able to predict the answers to these questions before new systems are developed and emplaced.

Performance prediction for an acoustic surveillance system requires models for both target signals and ambient noise. By noise characteristics we mean those statistics of the noise which relate to system performance measures. In order to determine what noise statistics are desired, we look at several performance-related noise questions.

To do this we first look at the requirements for effective surveillance. In order to achieve satisfactory surveillance we must be able to detect the target for at least a short period of time. Moreover, these periods of detection must occur frequently enough to maintain satisfactory surveillance. In order to be able to answer this question we may first formulate a corresponding question about the noise at a receiving point: What are the chances that the averaged squared noise pressure will be below some threshold X for at least M minutes at least T times per day?

The complete solution to this problem is extraordinarily difficult and generally not feasible since it requires an extraordinarily high-order characterization of the noise random process. Performance prediction models that are currently available use the sonar equation and an assumption that the averaged squared pressure of the ambient noise has a Gaussian distribution with fixed parameters. The noise level, however, fluctuates, and this characterization using fixed parameters has been inadequate for predicting the performance of current systems. In future systems with high spectral and/or spatial resolution, a simple model such as this would be even less adequate since high resolution implies less averaging which will make the distributions of the averaged squared noise pressure even less Gaussian.

Now, knowing the question we would like to be able to answer with the performance prediction model and the fact that the current techniques do not permit an adequate characterization of the effects of fluctuation, we may proceed to consider a hierarchy of problems.

The first problem is concerned with calculating the probability that the noise will be sufficiently low over a short period of time to allow a valid target detection. In both single and multiple array surveillance systems we require that a target be detected some minimum number of times within several successive averaging periods of the detection system. The simplest corresponding noise problem is to calculate the probability that the noise intensity remains below some threshold at least two times within several

successive averaging periods. From this we may then calculate the probabilities that it is below threshold n times out of m samples by making some assumptions on the structure of the random process (such as the assumption of a first-order Markov process). A second question concerns the frequency of target detections. One way this may be evaluated is to first calculate a relaxation time. At intervals equal to or greater than the relaxation time, samples of the noise will be independent, or approximately so. If a target is detected at some time then the probability that it is detected again at intervals greater than the relaxation time is simply equal to the probability of detection; i.e., the probability of target detection after intervals equal to or greater than the relaxation time has passed does not depend upon whether or not the target was detected at time zero.

These two questions are concerned with time-dependent characterizations of the noise intensity. Measurements of these parameters are quite difficult since extensive data must be collected to validate the parameters. It is thus also useful to consider several time-independent questions. The first of these concerns calculating the probability density of the averaged squared noise pressure, which can then be used in establishing the ROC curve for the system. Finally, we may wish to calculate the mean received noise intensity level.

Proceeding from the more complicated probability measures to the simplest probability measures, we see that the first question may be answered with a second-order density function. A second-order density function is simply the joint probability density of the averaged squared noise pressure at some time and its value τ time units later. This assumes, of course, that

the process is stationary. Relaxation times are typically evaluated from the covariance coefficient function. We define the relaxation time as that value of τ for which the covariance coefficient function equals a specified fractional value. We may also desire relaxation times computed from other statistics. For example, we may want the relaxation time associated with low-noise periods. At most, the time independent problems require that we have an estimate of the probability density function of the averaged squared noise pressure; for application in the sonar equation the required measure is simply the mean noise level. We note that all of the above measures may be calculated from the second-order probability density. A summary of the required statistical measures is given in Table 1.1.

Table 1.1: Required Statistical Measures

Probability Measure	Example(s) of Applications
$d(x, x_\tau)$	Short-Term Statistics of Low-Noise Events
$\mathrm{Cov}\ (X, X_\tau)$	Experimental Design, Cumulative Probability of Detection Models
$d(x)$ for $E(X^2)$, $E(X)$	Detection Performance Under Variability
$E(X)$	Sonar Equation

In the next section, the basis for predicting the averaged squared noise pressure resulting from discrete noise sources is derived.

1.2 Averaged Squared Pressure

The most frequently measured noise statistic is the averaged squared pressure in a given frequency passband

$$\text{[illegible]}) = T^{-1} \int_{t-T}^{t} P^2(u)\, du \qquad (1\text{-}1)$$

where T is the averaging period

P(t) is the instantaneous sound pressure at the point of observation

The sound pressure at a point resulting from a collection of point sources can be expressed as

$$P(t) = \sum_i w_i(t) U_i(t-\tau_i) \qquad (1\text{-}2)$$

where $w_i(t)$ is the amplitude transmission factor from the $i^{\underline{th}}$ source to the receiving point

$U_i(t)$ is a zero mean stationary random process representing the pressure at a unit distance from the $i^{\underline{th}}$ source. $U_i(t)$ is statistically independent of $U_j(t)$, $j \neq i$.

τ_i is the propagation time from the $i^{\underline{th}}$ source to the observation point

Equation (1-2) is a consequence of the principal of superposition of the instantaneous pressures of the sound waves from multiple point sources.

Substituting (1-2) in (1-1) gives

$$X(t) = \sum_i \sum_j T^{-1} \int_{t-T}^{t} du\ w_i(u) w_j(u) U_i(u-\tau_i) U_j(u-\tau_j) \qquad (1\text{-}3)$$

If the transmission factors do not change appreciably during the averaging period, then

$$X(t) \approx \sum_i \sum_j w_i(t) w_j(t) T^{-1} \int_{t-T}^{t} du\ U_i(u-\tau_i) U_j(u-\tau_j) \qquad (1\text{-}4)$$

If the averaging time is large compared to the reciprocal of the width of the observation passband, then

$$T^{-1} \int_{t-T}^{t} du\ U_i(u-\tau_i) U_j(u-\tau_j) \approx S_i, \quad i = j \qquad (1\text{-}5)$$

$$\approx 0, \quad i \neq j \qquad (1\text{-}6)$$

where S_i is the mean square pressure at unit distance from the $i^{\underline{th}}$ source

Applying (1-5) and (1-6) in (1-4) gives

$$X(t) \approx \sum_i z_i(t) S_i \qquad (1\text{-}7)$$

where $z_i(t) = w_i^2(t)$.

The result (1-7) is the basis used for the calculation of averaged squared pressure. In essence, this is the basis for the calculations of Goldman*, and Marshall and Cornyn.† The next subsection concerns the application of (1-7) to the prediction of statistical measures of shipping noise.

1.3 Approach

In a band of rather low frequencies, the ambient noise in the ocean is primarily generated by ship traffic. If the squared noise pressure in this band is monitored at a point and a short-term (on the order of a minute) running average is obtained, it would be found that the running average fluctuates with time in an unpredictable manner. It is thus reasonable to consider the averaged squared noise pressure at a point as a random variable X characterized by a probability density function. Although this density function contains information about the variability of X, it gives no statistical information about its time variation.

---

*J. Goldman, "OSTP-31JG: A Model of Broadband Ambient Noise Fluctuations due to Shipping (U)," Bell Laboratories, September 1974, CONFIDENTIAL.

†S. W. Marshall, J. J. Cornyn, Ambient Noise Prediction, Vol. 1 – Model of Low-Frequency Ambient Sea Noise, NRL Report No. 7755, June 1974.

If X_τ represents observations taking place at τ time units after observations X, then the joint probability density of X and X_τ contains information about the average time variation of X. From this joint density, lower-order statistical measures can be derived. One of these is the autocovariance function, which is the expected value of the random variable $(X-m_x)\ (X_\tau-m_x)$, where m_x is the average value of X. Also, the density of X is one of the marginal densities of the joint density.

In order to predict surveillance system performance, the directional characteristics of shipping noise must also be considered. For a first level of approximation, this can be done by predicting the noise arriving from ships within suitably narrow azimuth sectors.

Some of the elements involved in the approach are depicted in Figure 1.1. The receiving point of interest might be the site of a sensor, or a site being considered. This receiving point is in an acoustic basin defined by bathymetry (e.g., land masses and high underwater ridges). The sound intensity from sources outside of the basin will be considered negligible at the interior points.

For reasonable periods of time, the merchant ship traffic will occur within rather well-defined route envelopes. Sometimes, for political or economic reasons, the routes and the traffic on the routes can change abruptly. When such changes occur, the calculation program can be employed to make new noise predictions.

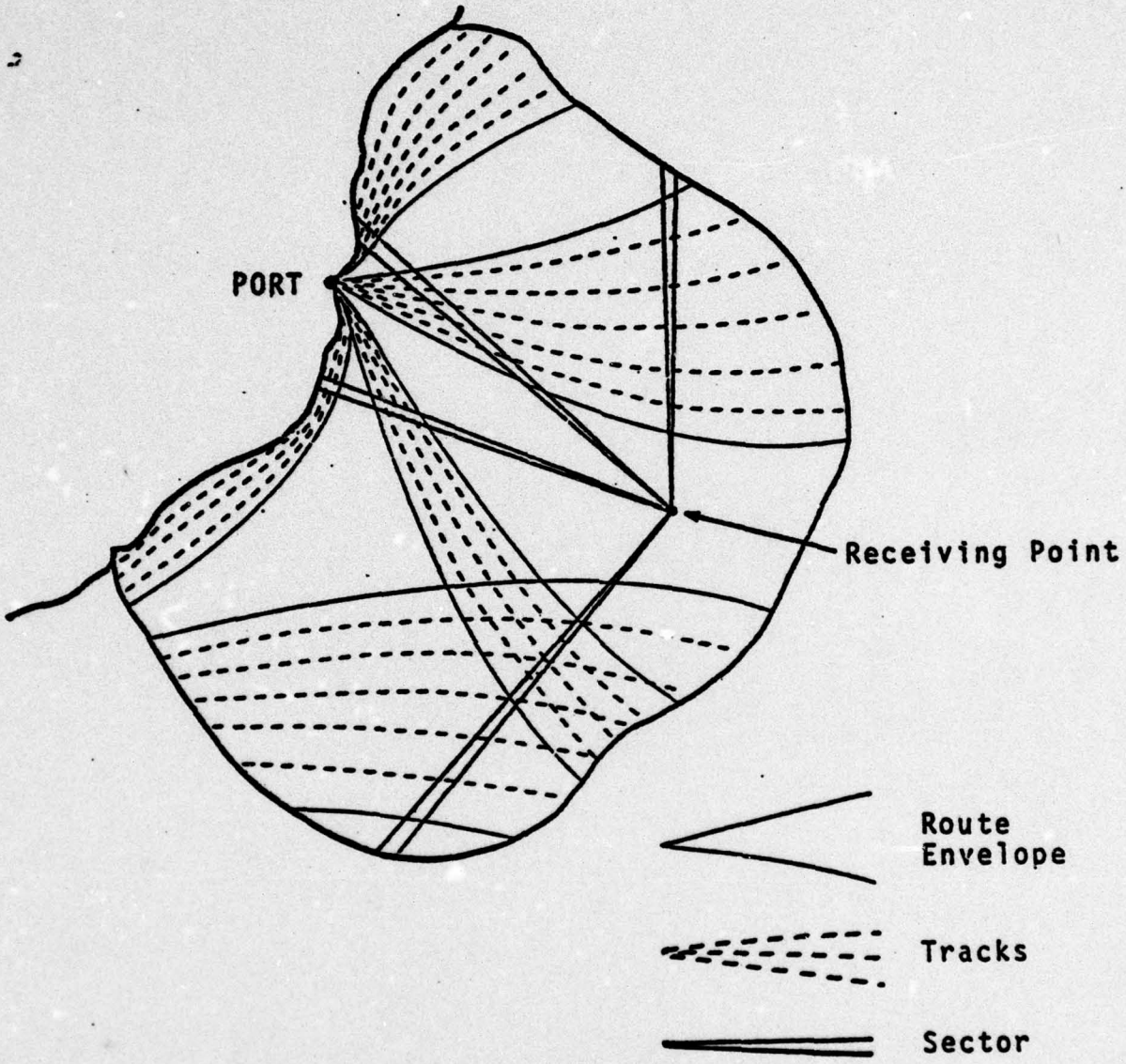

FIGURE 1.1 BASIN CONCEPT

Figure 1.1 shows four narrow azimuth sectors, none of which intercepts all of the route envelopes. In brief, the approach for a given sector is to calculate the joint probability density of X and X_τ based on the traffic statistics of route envelopes that intercept the sector. Also required are the acoustic source characteristics of ships on the routes, and the acoustic transmission loss function for the sector.

The received noise intensity will fluctuate for several reasons. One is the movement of the ships in and out of the sector. Another is the variation of transmission loss as ships move along their tracks within the sector. The extent and rate of possible variation can be fairly large. For example, in the vicinity of a convergence zone, the transmission loss can vary over an interval as great as 15 dB in a range increment of a few miles.

For noise in narrow frequency bands, additional variability results from the narrowband components of the noise radiated by the ships. This is because the frequency of those components varies from ship to ship.

The derivation of the joint density is organized according to the routes that cross the specified sector, and by the ship types on these routes. Figure 1.2 illustrates the intersection of a sector by one route envelope. For the calculation, we need only account for those ships that are in the sector at some time during the period τ. At the initial observation time, these ships are included in an area that is somewhat larger than the intersection of the sector and the route envelope. This part of the route envelope will be termed the area of interest.

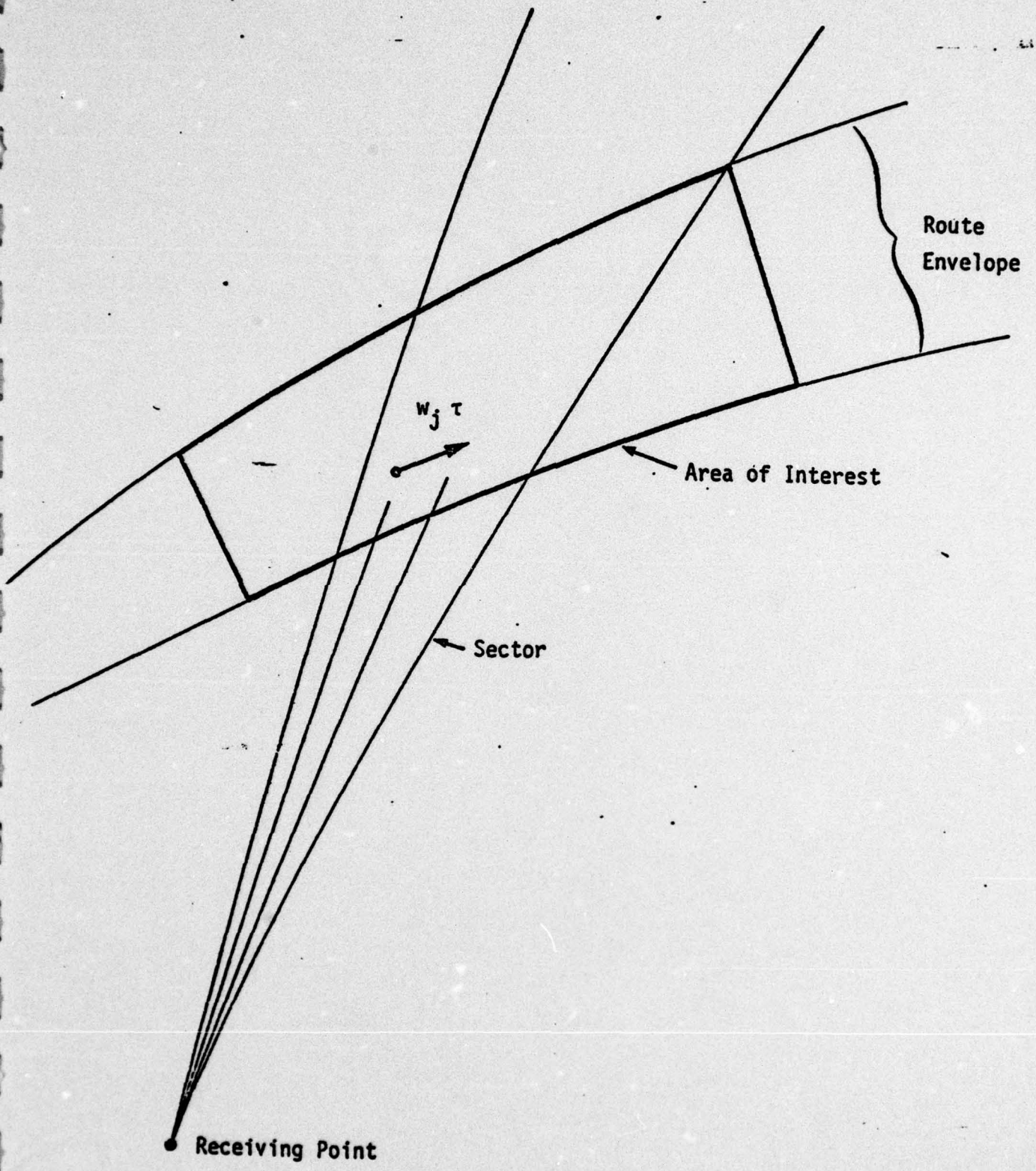

FIGURE 1.2 INTERSECTION OF A SECTOR WITH A ROUTE ENVELOPE

For the initial observation, the sound intensity at the receiving point resulting from all of the ships in the sector can be expressed as

$$X = \sum_{i=1}^{m} \sum_{j=1}^{n} \sum_{k=1}^{A_{ij}} S_{ijk} Z_{ijk} \qquad (1\text{-}8)$$

where m is the number of routes crossing the sector,

n is the number of ship types,

A_{ij} is the number of ships of type j on route i in the region of interest in the beginning of the period; A_{ij} is a random variable,

S_{ijk} is the source intensity of the $k^{\underline{th}}$ ship of type j in the region of interest of route i; it is a random variable that is statistically independent of the source intensity of any other ship.

The power transmission factor from ship ijk to the receiving point at the beginning of the period is

$$Z_{ijk} = z(G_{ijk}, Q_{ijk}) \qquad (1\text{-}9)$$

where z( ) is a deterministic power transmission function appropriate to the sector; outside of the sector its value is zero.

G_{ijk} is the longitudinal coordinate (in the direction of travel) of ship ijk at the beginning of the period; it is a random variable that is statistically independent of the coordinate of any other ship.

Q_{ijk} is the transverse coordinate (normal to the direction of travel) of ship ijk at the beginning of the period; it is a random variable that is statistically independent of the transverse coordinate of any other ship, and of the longitudinal coordinates of all ships.

At a time τ units later, the sound intensity at the receiving point resulting from ships in the sector is

$$X_\tau = \sum_{i=1}^{m} \sum_{j=1}^{m} \sum_{k=1}^{A_{ij}} S_{ijk} Z_{\tau ijk} \qquad (1\text{-}10)$$

where

$$Z_{\tau ijk} = z(G_{ijk} + w_j \tau, Q_{ijk}) \qquad (1\text{-}11)$$

w_j is the speed of the ships of type j. The appearance of the random variable A_{ij} (definition on previous page) in both (1-8) and (1-10) does not imply that the number of ships in the intersection of the observation sector and the route envelope is necessarily the same at the two observation times. The factor Z_{ijk} nullifies the contributions of ships outside of the sector at the beginning of the observation period, and the factor $Z_{\tau ijk}$

nullifies the contributions of those ships that are outside of the sector τ units later.

Equations (1-8) and (1-10) are the bases for calculating the joint characteristic function for X and X_τ.

2.0 THE JOINT CHARACTERISTIC FUNCTION

2.1 Derivation

The joint probability density function for X and X_τ can be obtained from the joint characteristic function, which is derived in this section.

The joint characteristic function for X and X_τ is

$$\Phi_{XX_\tau}(\alpha,\beta) = E[\exp j(\alpha X + \beta X_\tau)] \tag{2-1}$$

Substituting (1-8) and (1-10) in (2-1) and gives

$$\Phi_{XX_\tau}(\alpha,\beta) = E\left\{\exp j\left[\sum_{i=1}^{m}\sum_{j=1}^{n}\sum_{k=1}^{A_{ij}} S_{ijk}\left(\alpha Z_{ijk} + \beta Z_{\tau ijk}\right)\right]\right\} \tag{2-2}$$

$$= E\left\{\prod_{i=1}^{m}\prod_{j=1}^{n}\prod_{k=1}^{A_{ij}} \exp j\, S_{ijk}\left(\alpha Z_{ijk} + \beta Z_{\tau ijk}\right)\right\} \tag{2-3}$$

$$= \prod_{i=1}^{m}\prod_{j=1}^{n} \Phi_{ij}(\alpha,\beta) \tag{2-4}$$

where

$$\Phi_{ij}(\alpha,\beta) = E\left\{\prod_{k=1}^{A_{ij}} \exp j\, S_{ijk}\left(\alpha Z_{ijk} + \beta Z_{\tau ijk}\right)\right\} \tag{2-5}$$

Performing the expectation operation in (2-5) gives

$$\Phi_{ij}(\alpha,\beta) = \sum_{a=0}^{\infty} p_{ij}(a)\left[\int dg f_{G_i}(g)\int dq f_{Q_i}(q)\int ds f_{S_j}(s)\exp js\left(\alpha z_{ij} + \beta z_{\tau ij}\right)\right]^a \tag{2-6}$$

where $p_{ij}(a) = P(A_{ij} = a)$, $a = 0, 1, 2, 3, \ldots$

$f_{G_i}(\ )$ is the probability density function for G_{ijk}; $j = 1, 2, \ldots, n$; $k = 1, 2, 3, \ldots$

$f_{Q_i}(\ )$ is the probability density function for Q_{ijk}; $j = 1, 2, \ldots, n$; $k = 1, 2, 3, \ldots$

The inner integral can be expressed as a characteristic function; thus

$$\Phi_{ij}(\alpha,\beta) = \sum_{a=0}^{\infty} p_{ij}(a)\left[\int dg f_{G_i}(g)\int dg f_{Q_i}(q)\Phi_{S_j}\left(\alpha z_{ij} + \beta z_{\tau ij}\right)\right]^a \tag{2-7}$$

In the sequel, it is assumed that A_{ij} is a Poisson random variable*; thus, its probabilities are given by

$$p_{ij}(a) = \exp(-a_{ij})a_{ij}^a \div a!,\ a = 0, 1, 2, 3, \ldots \tag{2-8}$$

*This assumption is discussed in Appendix B.

where a_{ij} is the average number of ships of type j in an increment of route i.

Substituting (2-8) into (2-7) gives

$$\Phi_{ij}(\alpha,\beta) = \exp(-a_{ij}) \sum_{a=0}^{\infty} \left[a_{ij} \int dg f_{G_i}(g) \int dq f_{Q_i}(q) \Phi_{S_j}\left(\alpha z_{ij} + \beta z_{\tau ij}\right)\right]^a \div a! \tag{2-9}$$

The sum is the power series expansion for the exponential of the quantity in brackets; thus

$$\Phi_{ij}(\alpha,\beta) = \exp(-a_{ij}) \exp\left[a_{ij} \int dg f_{G_i}(g) \int dq f_{Q_i}(q) \Phi_{S_j}\left(\alpha z_{ij} + \beta z_{\tau ij}\right)\right] \tag{2-10}$$

The second characteristic function is

$$\Psi_{ij}(\alpha,\beta) \overset{\Delta}{=} \ln \Phi_{ij}(\alpha,\beta)$$

$$= -a_{ij} + a_{ij} \int dg f_{G_i}(g) \int dq f_{Q_i}(q) \Phi_{S_j}\left(\alpha z_{ij} + \beta z_{\tau ij}\right) \tag{2-11}$$

The region of integration is, in effect, the region of interest depicted in Fig. 1.2. This region can be divided into two regions: the first (R_1) being the intersection of the observation sector and the region of interest, and the second (R_2) is the remainder of the region of interest. Let

$$F_{ij}(\alpha,\beta) = \int dg \int_{R_1} dg f_{G_i}(g) f_{Q_i}(q)\, \Phi_{S_j}\left(\alpha z_{ij} + \beta z_{\tau ij}\right) \qquad (2\text{-}12)$$

and $G_{ij}(\alpha,\beta)$ be the corresponding integral over R_2. Since both z_{ij} and $z_{\tau ij}$ are taken as zero outside the sector, it is seen that

$$G_i(\alpha,\beta) = G_{ij}(0, 0) \qquad (2\text{-}13)$$

Substituting (2-12) and (2-13) in (2-11) gives

$$\Psi_{ij}(\alpha,\beta) = -a_{ij} + a_{ij}\left[F_{ij}(\alpha,\beta) + G_{ij}(0, 0)\right] \qquad (2\text{-}14)$$

Since $\Psi_{ij}(0, 0) = 0$, evaluation of (2-14) at 0, 0 yields

$$-a_{ij} + a_{ij}G(0, 0) = -a_{ij}F_{ij}(0, 0) \qquad (2\text{-}15)$$

Substituting this result in (2-14) yields

$$\Psi_{ij}(\alpha,\beta) = a_{ij}\left[F_{ij}(\alpha,\beta) - F_{ij}(0, 0)\right] \qquad (2\text{-}16)$$

If the distributions of the longitudinal coordinates G_{ijk} are uniform in the region of interest, then

$$f_{G_i}(g) = (g_2 - g_1)^{-1}, \quad g_1 \le g \le g_2 \qquad (2\text{-}17)$$

$$= 0, \text{ elsewhere} \qquad (2\text{-}18)$$

and

$$\Psi_{ij}(\alpha,\beta) = \rho k_{ij}\left[H_{ij}(\alpha,\beta) - H_{ij}(0, 0)\right] \qquad (2\text{-}19)$$

where $k_{ij} = a_{ij} + (g_2 - g_1)\rho$ is the average number of ships of type j on route i per unit distance on the earth's surface

ρ is the radius of the earth

$$H_{ij}(\alpha,\beta) = \int_{R_1} dg \int dq f_{Q_i}(q) \Phi_{S_j}\left(\alpha z_{ij} + \beta z_{\tau ij}\right) \qquad (2\text{-}20)$$

Taking the natural logarithm of (2-4) gives the second characteristic function for X and X_τ:

$$\Psi_{XX_\tau}(\alpha,\beta) = \sum_{i=1}^{m} \sum_{j=1}^{n} \Psi_{ij}(\alpha,\beta) \qquad (2\text{-}21)$$

where the terms $\Psi_{ij}(\alpha,\beta)$ are given by (2-19) in which the function $H_{ij}(\alpha,w)$ is given by (2-20).

2.2 Relationship of Coordinates

One of the principal results of the previous section is (2-20), in which the variables of integration are the route coordinates g and q. However, the power transmission functions z and z_τ are functions of the observation variables related to range and bearing. To perform this calculation, the relationship between the sets of variables must be defined.

Figure 2.1 shows the spherical coordinate system. All of the lines are arcs of great circles, and the reference point R is the intersection of the nominal route and the center of the observation sector. Points O and S mark the locations of the observation point and a ship, respectively. The surface angle F is the orientation of the centerline of the sector with respect to the nominal route. The earth-centered angle g is the angular displacement of the ship along the nominal route, and the earth centered angle q is the displacement of the ship from the route. The surface angle D is the displacement of the line of observation from the centerline of the sector. The earth-centered angles s and r are the displacements of the reference point and the ship from the observation point, respectively.

The approach that was chosen was to employ the observation variables r and D as the variables of integration. The equivalent to (2-20) is then

$$H_{ij}(\alpha,\beta) = \int dD \int dr |J(r,D)| f_{Q_i}(q)\, \Phi_{S_j}\left(\alpha z_{ij} + \beta z_{\tau ij}\right) \qquad (2\text{-}22)$$

In Appendix A it is shown that the Jacobian for the specified pairs of variables is

$$J = \sin r \div \cos q \qquad (2\text{-}23)$$

where

$$\sin q = \sin r \sin D \cos F + (\cos s \sin r \cos D - \sin s \cos r) \sin F \qquad (2\text{-}24)$$

$$\simeq D \sin r \cos F + \sin(r - s) \sin F,\ D \leq \pi/18 \qquad (2\text{-}25)$$

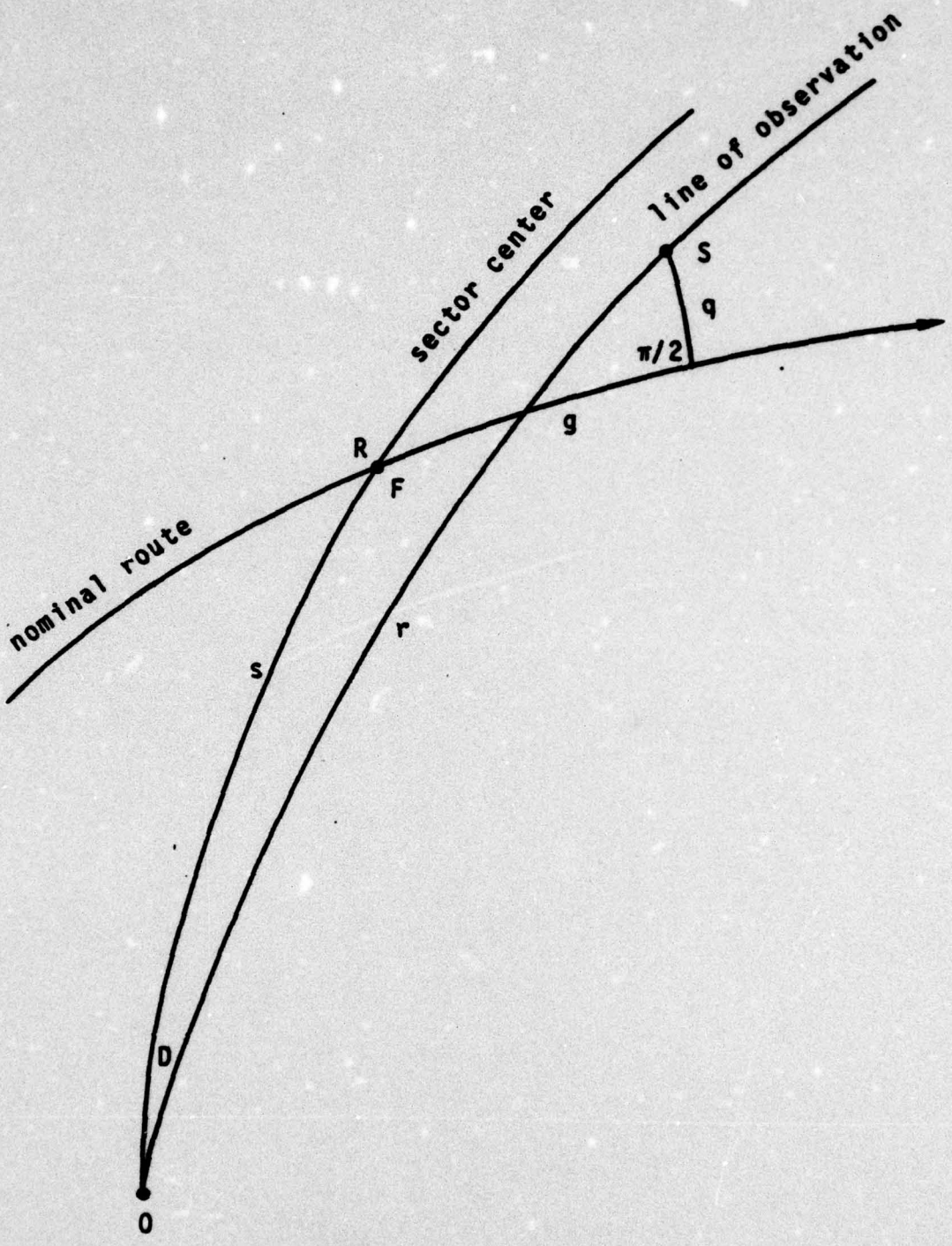

FIGURE 2.1 COORDINATE SYSTEM

Either (2-24) or (2-25) could be used to generate the denominator of (2-23) and the argument of $f_{Q_1}(\ )$ in (2-22). For routes that are narrow, sin q $\simeq$ q, and cos q $\simeq$ 1, and substituting the latter in (2-23) gives

$$J \simeq \sin r \tag{2-26}$$

It is also required to determine the limits of integration on r for a given value of D. One approach is to first determine the limits for D = 0. The solution of (2-24) for the case is

$$\sin (r - s) = \sin q_b \div \sin F \tag{2-27}$$

For the next value of D, the solutions of (2-27) would be the first trial solutions to be employed in (2-24) or (2-25). The next set of trial solutions would be selected on the basis of the surface angle F. For example, if D is positive, and F is larger than 90 degrees, then the trial solutions would be one increment of r greater than the initial solutions. For the next value of D, the first trial solutions would be the values of r found for the previous value of D.

3.0 FOURIER TRANSFORM ALGORITHMS FOR LOGARITHMICALLY SAMPLED DATA

This section presents numerical algorithms for computing one-dimensional Fourier transforms, one-dimensional inverse Fourier transforms and two-dimensional inverse Fourier transforms of logarithmically sampled data.

The characteristic function $\Phi(w)$ of a probability density function $f(x)$ is defined* as the Fourier transform

$$\Phi_x(w) = \int_{-\infty}^{+\infty} f(x)\, e^{-jwx}\, dx \qquad (3\text{-}1)$$

where w = radians/unit of x.

The probability density function can be obtained from the characteristic function by the inverse Fourier transform

$$f(x) = \frac{1}{2\pi} \int_{-\infty}^{+\infty} \Phi_x(w)\, e^{jwx}\, dw \qquad (3\text{-}2)$$

The joint probability density function $f(x,y)$ of two random variables x and y can be obtained from the joint characteristic function $\Phi_{xy}(\alpha,\beta)$ by the two dimensional inverse Fourier transform

*A. Papoulis, "Probability, Random Variables and Stochastic Processes," McGraw-Hill, 1965.

$$f(x,y) = \frac{1}{4\pi^2} \int_{-\infty}^{+\infty} \int_{-\infty}^{+\infty} \Phi_{xy}(\alpha,\beta)\, e^{j\alpha x + j\beta y}\, d\alpha\, d\beta \qquad (3\text{-}3)$$

where α = radians/unit of x,
β = radians/unit of y.

3.1 Fourier Transform Algorithm

Given the probability density function f(x) in the form

$$f(x) = \zeta\delta(x) + g(x) \qquad (3\text{-}4)$$

where $\delta(x)$ is the unit impulse function, ζ is a constant, possibly zero, and g(x) is piecewise-continuous, the characteristic function from Equation (3-1) becomes

$$\Phi_x(w) = \xi + \int_{-\infty}^{+\infty} g(x)\, e^{-jwx}\, dx \qquad (3\text{-}5)$$

The form of the probability density function of Equation (3-4) allows for an impulse at the origin. Thus, the constant ζ is the probability that x has the value zero. Assuming g(x) is only non-zero in the range x = 1 to x = x_0 and using Euler's identity, Equation (3-5) can be written in terms of its real and imaginary parts as

$$R(w) = \zeta + \int_{x=1}^{x=x_0} g(x) \cos wx\, dx \qquad (3\text{-}6)$$

and

$$I(w) = -\int_{x=1}^{x=x_0} g(x) \sin wx \, dx \qquad (3\text{-}7)$$

where $\Phi_x(w) = R(w) + jI(w)$, and $j = \sqrt{-1}$.

Assume the function g(x) has known values only at the points g[x(n)], where x is sampled logarithmically at one-fourth dB intervals, that is $x(n) = 10^{n/40}$, for n = 0, 1, 2, ..., N. Note that the first sample is at x(0) = 1.0 and the last at $x(N) = x_0$. Hence, there will be N + 1 sample points for the function g(x(n)). For example, if g(x) has a non-zero range of x = 1 to 10^6, then 241 sample points will be used to describe g(x). The advantage of logarithmically spaced sample points is apparent from this example, since we need only 241 points to represent a dynamic range of one million. However, although the function g(x) can vary rapidly at smaller values of x, it must be very slowly changing at the larger values of x for this sampling scheme to be valid. Since the types of probability density functions involved in ambient noise modelling fall into this category, logarithmic sampling is appropriate for this application.

Standard FFT algorithms cannot be used since the sampling is not uniform. A new algorithm is developed to numerically evaluate the integrals in Equations (3-6) and (3-7).

It is assumed that g(x) is piecewise-linear over each interval and can be represented, as in Figure 3.1, as a series of straight lines between sample points.

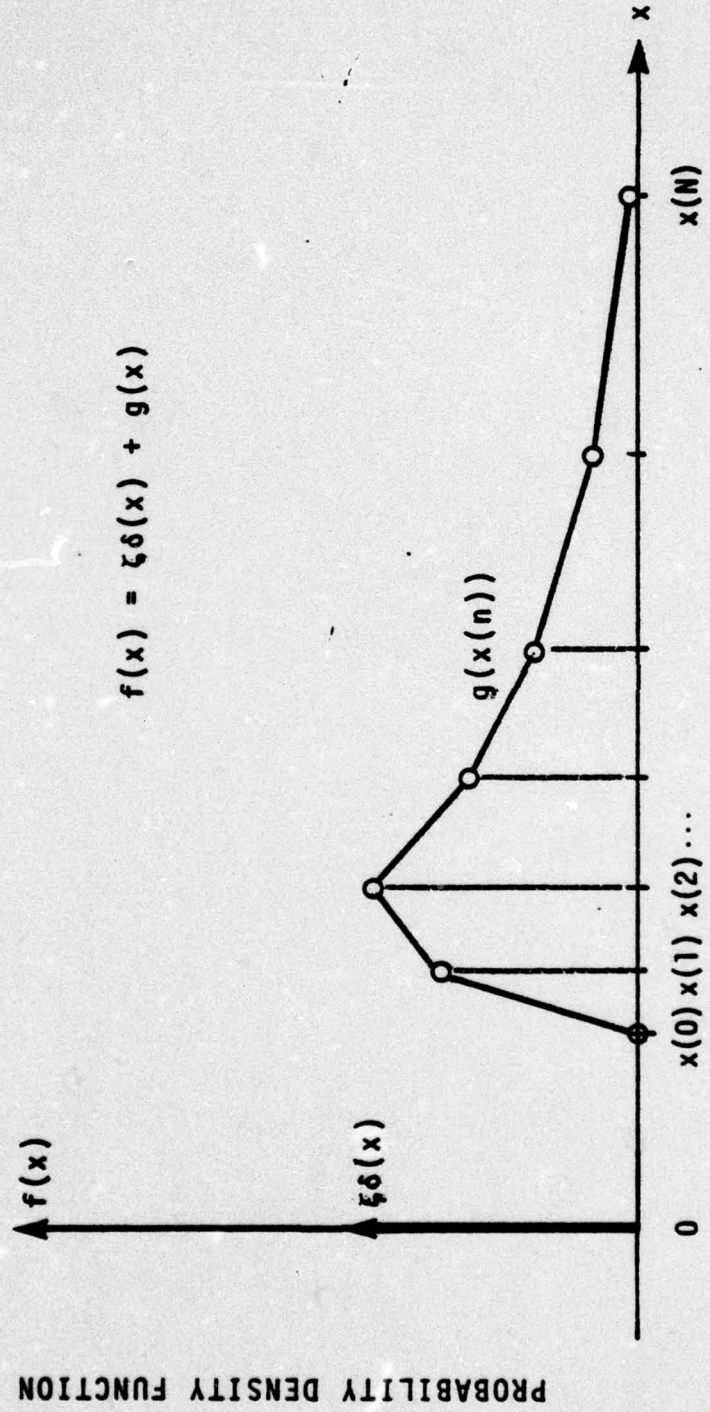

FIGURE 3.1 PIECEWISE-LINEAR APPROXIMATION OF PROBABILITY DENSITY FUNCTION

The function g(x) can be approximated as the sum of the individual straight lines in each segment. Figure 3.2 shows one such general interval between sample points. From Figure 3.2, the equation for the straight line in the $n^{\underline{th}}$ interval is

$$g_n(x) = \begin{cases} \left[\frac{g[x(n+1)] - g[x(n)]}{x(n+1) - x(n)}\right] x + \left[\frac{x(n+1)g[x(n)] - x(n)g[x(n+1)]}{x(n+1) - x(n)}\right] \\ \qquad \text{for } x(n) \leq x \leq x(n+1) \\ 0 \text{ otherwise} \end{cases} \tag{3-8}$$

Hence, the approximation is

$$g(x) \cong \sum_{n=0}^{N-1} g_n(x) \tag{3-9}$$

Replacing g(x) in Equations (3-6) and (3-7) by Equation (3-9) and interchanging summation and integration gives the real and imaginary parts of the characteristic function

$$R(w) = \zeta + \sum_{n=0}^{N-1} \int_{x=x(n)}^{x(n+1)} g_n(x) \cos wx \, dx \tag{3-10}$$

$$I(w) = - \sum_{n=0}^{N-1} \int_{x=x(n)}^{x(n+1)} g_n(x) \sin wx \, dx \tag{3-11}$$

Substituting for $g_n(x)$ from Equation (3-8) and evaluating the integrals yields for the characteristic function

$$g_n(x) = \left[\frac{g[x(n+1)] - g[x(n)]}{x(n+1) - x(n)}\right] x + \left[\frac{x(n+1)g[x(n)] - x(n)g[x(n+1)]}{x(n+1) - x(n)}\right]$$

FIGURE 3.2 PIECEWISE-LINEAR APPROXIMATION FOR THE $n^{\underline{th}}$ INTERVAL

$$R[w(m)] = \zeta + \sum_{n=0}^{N-1} \Bigg\{ g[x(n+1)] \frac{\sin w(m)x(n+1)}{w(m)} - g[x(n)] \frac{\sin w(m)x(n)}{w(m)} + \frac{g[x(n+1)] - g[x(n)]}{w(m)} \left[\frac{\cos w(m)x(n+1) - \cos w(m)x(n)}{w(m)[x(n+1) - x(n)]} \right] \Bigg\} \tag{3-12}$$

and

$$I[w(m)] = -\sum_{n=0}^{N-1} \Bigg\{ g[x(n)] \frac{\cos w(m)x(n)}{w(m)} - g[x(n+1)] \frac{\cos w(m)x(n+1)}{w(m)} + \frac{g[x(n+1)] - g[x(n)]}{w(m)} \left[\frac{\sin w(m)x(n+1) - \sin w(m)x(n)}{w(m)[x(n+1) - x(n)]} \right] \Bigg\} \tag{3-13}$$

where w is sampled in the frequency domain as

$$w(m) = 10^{m/40}$$

for m = -N, -N+1, ..., -1, 0. Thus, there are the same number of sample points for w as for x.

Equations (3-12) and (3-13) can be further simplified, since certain terms cancel, and written in the form

$$R[w(m)] = \zeta - g[x(0)] \frac{\sin w(m)x(0)}{w(m)} + g[x(N)] \frac{\sin w(m)x(N)}{w(m)}$$

$$+ \frac{1}{w(m)} \sum_{n=0}^{N-1} \left\{ \left(g[x(n+1)] - g[x(n)] \right) \left(\frac{\cos w(m)x(n+1) - \cos w(m)x(n)}{w(m)[x(n+1) - x(n)]} \right) \right\} \quad (3\text{-}14)$$

and

$$I\left[w(m)\right] = g[x(N)] \frac{\cos w(m)x(N)}{w(m)} - g[x(0)] \frac{\cos w(m)x(0)}{w(m)}$$

$$- \frac{1}{w(m)} \sum_{n=0}^{N-1} \left\{ \left(g[x(n+1)] - g[x(n)] \right) \left(\frac{\sin w(m)x(n+1) - \sin w(m)x(n)}{w(m)[x(n+1) - x(n)]} \right) \right\} \quad (3\text{-}15)$$

for $m = -N, -N+1, \ldots, -1, 0$.

Equations (3-14) and (3-15) constitute the Fourier transform algorithm for logarithmically sampled data. This algorithm is used to compute the total radiated noise source characteristic function from the broadband and narrowband source density functions as described in Section 4.4.

Equations (3-14) and (3-15) can be made computationally efficient by pre-computing the [cos w(m)x(n+1) - cos w(m)x(n)] factor and the [sin w(m)x(n+1) - sin w(m)x(n)] factor for the range of values on m and n. These act as weighting coefficients, need be computed only once, and are stored in an array that can be called when needed in the calculations. It will be seen that this weighting coefficient array can be used in other parts of the computations.

In order to evaluate the accuracy of the Fourier transform algorithm described above, a test case was run on the computer. The test case was a uniform density function given by

$$f(x) = \begin{cases} 1.\ 10101 \times 10^{-4}, \text{ for } 100 \leq x \leq 10{,}000 \\ 0 \text{ otherwise} \end{cases} \qquad (3\text{-}16)$$

The actual Fourier transform of this uniform density function is

$$R(w) = \frac{\sin(10{,}000\ w) - \sin(100\ w)}{(9{,}900)\ w} \qquad (3\text{-}17)$$

for the real part and

$$I(w) = \frac{\cos(10{,}000\ w) - \cos(100\ w)}{(9{,}900)\ w} \qquad (3\text{-}18)$$

for the imaginary part.

Figures 3.3 and 3.4 show plots of the actual values and computed values for the real and imaginary parts, respectively. The computed values agree fairly well with the actual curve.

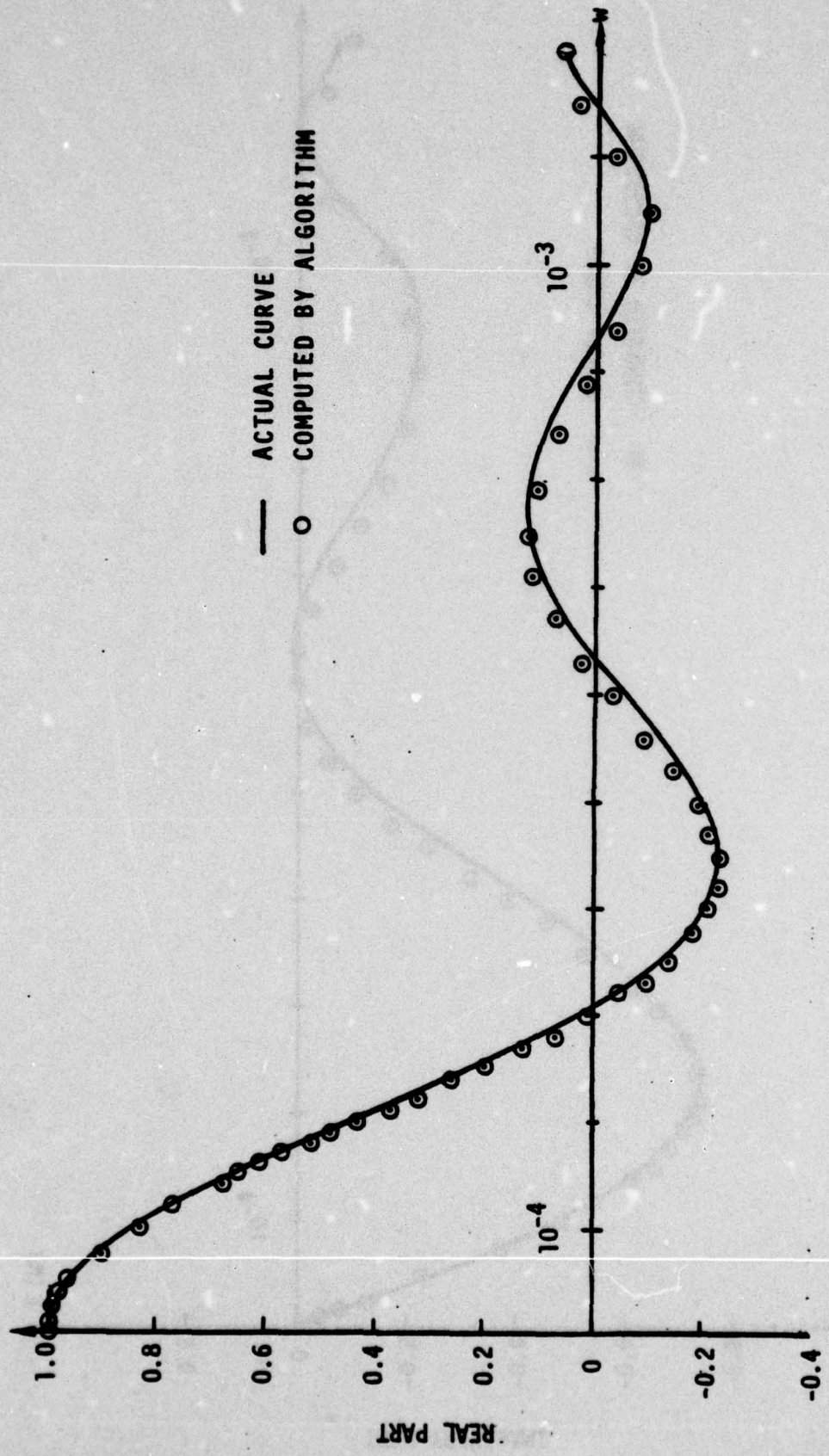

FIGURE 3.3 ACCURACY OF FOURIER TRANSFORM ALGORITHM; REAL PART OF FOURIER TRANSFORM OF UNIFORM DENSITY FUNCTION

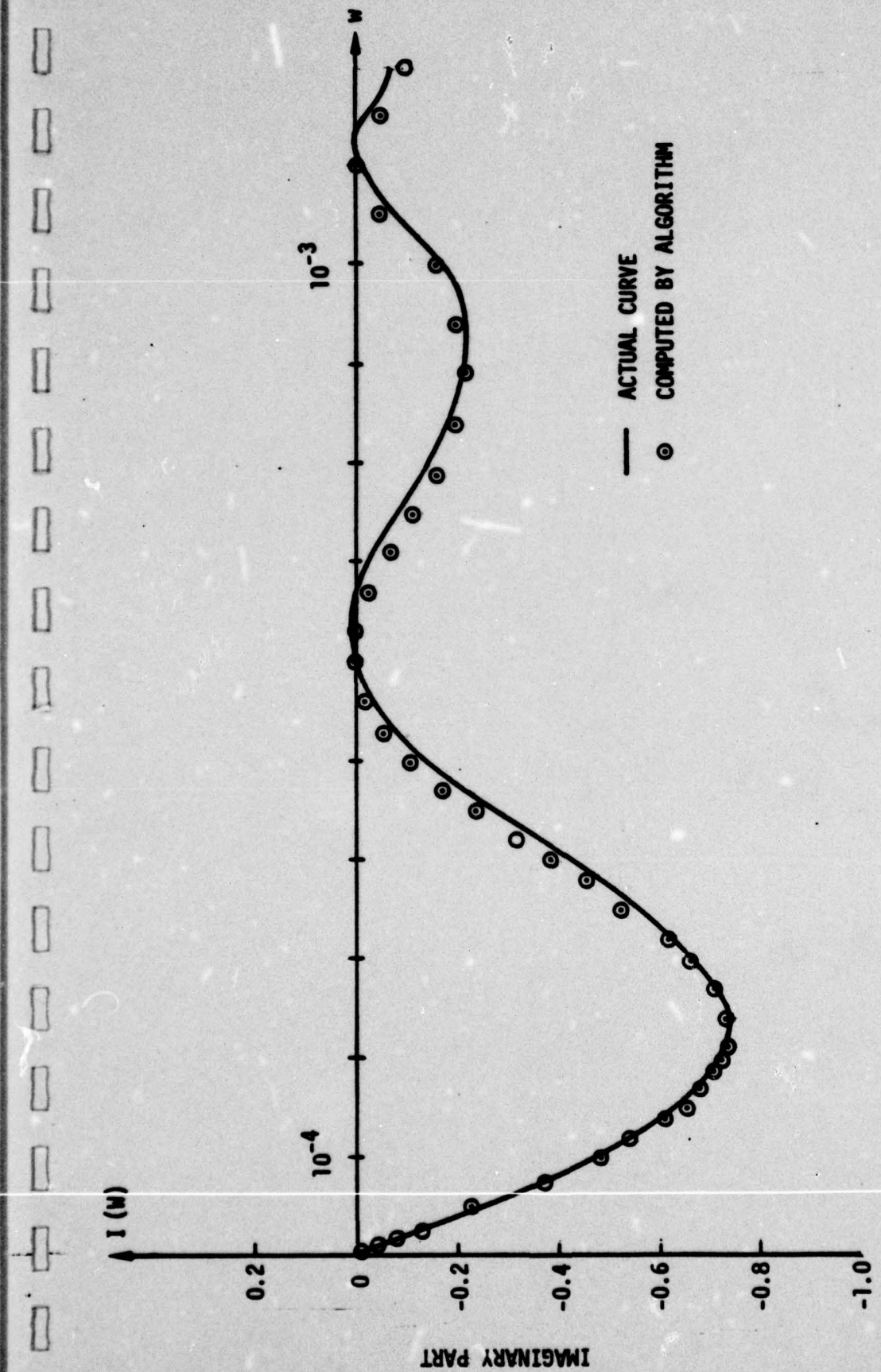

FIGURE 3.4 ACCURACY OF FOURIER TRANSFORM ALGORITHM: IMAGINARY PART OF FOURIER TRANSFORM OF UNIFORM DENSITY FUNCTION

The percent error remains within 10% over most of the range of the function.

3.2 Inverse Fourier Transform

In Section 2, the equation for the joint characteristic function was given in terms of the two frequency variables α and β. If β is set equal to zero, the joint characteristic function reduces to the characteristic function of received noise. An inverse Fourier transform algorithm for logarithmically sampled data is developed in this sub-section for computing the probability density function of received noise from the characteristic function.

Assume the characteristic function has the form:

$$\Phi_X(w) = R(w) + \zeta + j\, I(w) \qquad (3\text{-}19)$$

where ζ is a constant, possibly zero, equal to the probability of x taking the value of zero; that is, ζ is the magnitude of an impulse at the origin in the density function. From the properties of characteristic functions (Papoulis, op. cit.) it follows that $|\Phi_X(w)| \leq 1$ for all w and $\Phi_X(0) = 1$. Therefore, $I(0) = 0$ and $R(0) = 1 - \zeta$. $R(w)$ is an even function and $I(w)$ is an odd function.

Substituting $\Phi_X(w)$ from Equation (3-19) into Equation (3-2), and making use of the properties of characteristic functions, the probability density function can be written as

$$f(x) = \zeta\delta(x) + \frac{1}{\pi}\int_0^{+\infty} \Big\{R(w)\cos wx - I(w)\sin wx\Big\}dw \qquad (3\text{-}20)$$

The first step in the algorithm is to subtract ζ from the real part of $\Phi_X(w)$ to obtain R(w).

Assume that R(w) and I(w) can be approximated as piecewise-linear functions over each sample interval, where the samples in the frequency domain are spaced logarithmically, as in the previous section, as

$$w(m) = 10^{m/40}, \quad m = -N, -N+1, \ldots, -1, 0.$$

For the general $m^{\underline{th}}$ interval, R(w) and I(w) are approximated by the straight lines

$$R_m(w) = \begin{cases} \left[\frac{R[w(m+1)] - R[w(m)]}{w(m+1) - w(m)}\right] w + \left[\frac{w(m+1)R[w(m)] - w(m)R[w(m+1)]}{w(m+1) - w(m)}\right] \\ \qquad \text{for } w(m) \leq w \leq w(m+1) \\ 0 \text{ otherwise} \end{cases} \tag{3-21}$$

and

$$I_m(w) = \begin{cases} \left[\frac{I[w(m+1)] - I[w(m)]}{w(m+1) - w(m)}\right] w + \left[\frac{w(m+1)I[w(m)] - w(m)I[w(m+1)]}{w(m+1) - w(m)}\right] \\ \qquad \text{for } w(m \leq w \leq w(m+1) \\ 0 \text{ otherwise} \end{cases} \tag{3-22}$$

Then R(w) and I(w) can be functionally represented as

$$R(w) \approx \sum_{m=-N}^{-1} R_m(w) \tag{3-23}$$

$$I(w) \approx \sum_{m=-N}^{-1} I_m(w) \tag{3-24}$$

Using Equations (3-23) and (3-24) for R(w) and I(w) in Equation (3-20) and interchanging summation and integration yields

$$f(x) \approx \zeta\delta(x) + \frac{1}{\pi} \int_{w=0}^{w(-N)} \left\{ R(w) \cos wx - I(w) \sin wx \right\} dw$$

$$+ \frac{1}{\pi} \sum_{m=-N}^{-1} \int_{w=w(m)}^{w(m+1)} R_m(w) \cos wx \, dw$$

$$- \frac{1}{\pi} \sum_{m=-N}^{-1} \int_{w=w(m)}^{w(m+1)} I_m(w) \sin wx \, dw \tag{3-25}$$

Each integral in Equation (3-25) can be evaluated by using Equations (3-21) and (3-22) for $R_m(w)$ and $I_m(w)$, and a linear approximation for the integral from w = 0 to w(-N). After appropriate cancellation of some terms and other simplifications, the approximation to the probability density function becomes

$$f[x(n)] \approx \zeta\delta(x)$$

$$+ \frac{1}{\pi x(n)} \left\{ \left[1 - \zeta - R\, w(-N)\right] \left[\frac{1 - \cos w(-N)x(n)}{w(-N)x(n)}\right] \right.$$

$$\left. - I\left[w(-N)\right] \frac{\sin w(-N)x(n)}{w(-N)x(n)} \right.$$

$$+ R[w(0)] \sin w(0)x(n) + I\left[w(0)\right] \cos w(0)x(n)$$

$$+ \sum_{m=-N}^{-1} \left\{ \left[\left[R\left[w(m+1)\right] - R\left[w(m)\right]\right] \left[\frac{\cos w(m+1)x(n) - \cos w(m)x(n)}{x(n)[w(m+1) - w(m)]}\right] \right.\right.$$

$$\left.\left. - \left(I\left[w(m+1)\right] - I\left[w(m)\right]\right) \left[\frac{\sin w(m+1)x(n) - \sin w(m)x(n)}{x(n)[w(m+1) - w(m)]}\right] \right\} \right\}$$

(3-26)

where $x(n) = 10^{n/40}$, for $n = 0, 1, 2, \ldots, N$.

Equation (3-26) is the algorithm for the inverse Fourier transform for logarithmically spaced data. It was used to compute the probability density function from the characteristic function of received noise as described in Section 5. Note that the [cos w(m+1)x(n) - cos w(m)x(n)] terms and [sin w(m+1)x(n) - sin w(m)x(n)] terms in Equation (3-26) are the same weighting coefficients as described in Section 3.1. Thus, the same weighting coefficient array is used for the Fourier transform algorithm and the inverse Fourier transform algorithm. This increases the efficiency of the computer programs.

The accuracy of the algorithm given by Equation (3-26) was evaluated by a test case run on the computer. The test function was a uniform distribution given by

$$f(x) = \begin{cases} 1.00001 \times 10^{-7}, \text{ for } 100 \leq x \leq 1.0 \times 10^{7} \\ 0 \text{ otherwise} \end{cases} \qquad (3\text{-}27)$$

The input to the algorithm was the characteristic function for this uniform distribution, which is

$$\Phi(w) = \frac{\sin (1 \times 10^{7} w) - \sin (100 w)}{9.99990 \times 10^{6} w} + j \left[\frac{\cos (1 \times 10^{7} w) - \cos (100 w)}{9.99990 \times 10^{6} w} \right] \qquad (3\text{-}28)$$

Figure 3.5 shows a plot of the actual and computed values of the uniform density function versus power. The calculated values were within $\pm$ 10% of the actual values for most of the significant range of the function.

3.3 Two-Dimensional Inverse Fourier Transform

The equation for the joint characteristic function of received noise, $\Phi_{XX_\tau}(\alpha,\beta)$, was developed in Section 2. A two-dimensional inverse Fourier transform algorithm for logarithmically sampled data is developed in this section. This algorithm can be used to compute the joint probability density function $f_{XX_\tau}(x,x_\tau)$ from $\Phi_{XX_\tau}(\alpha,\beta)$.

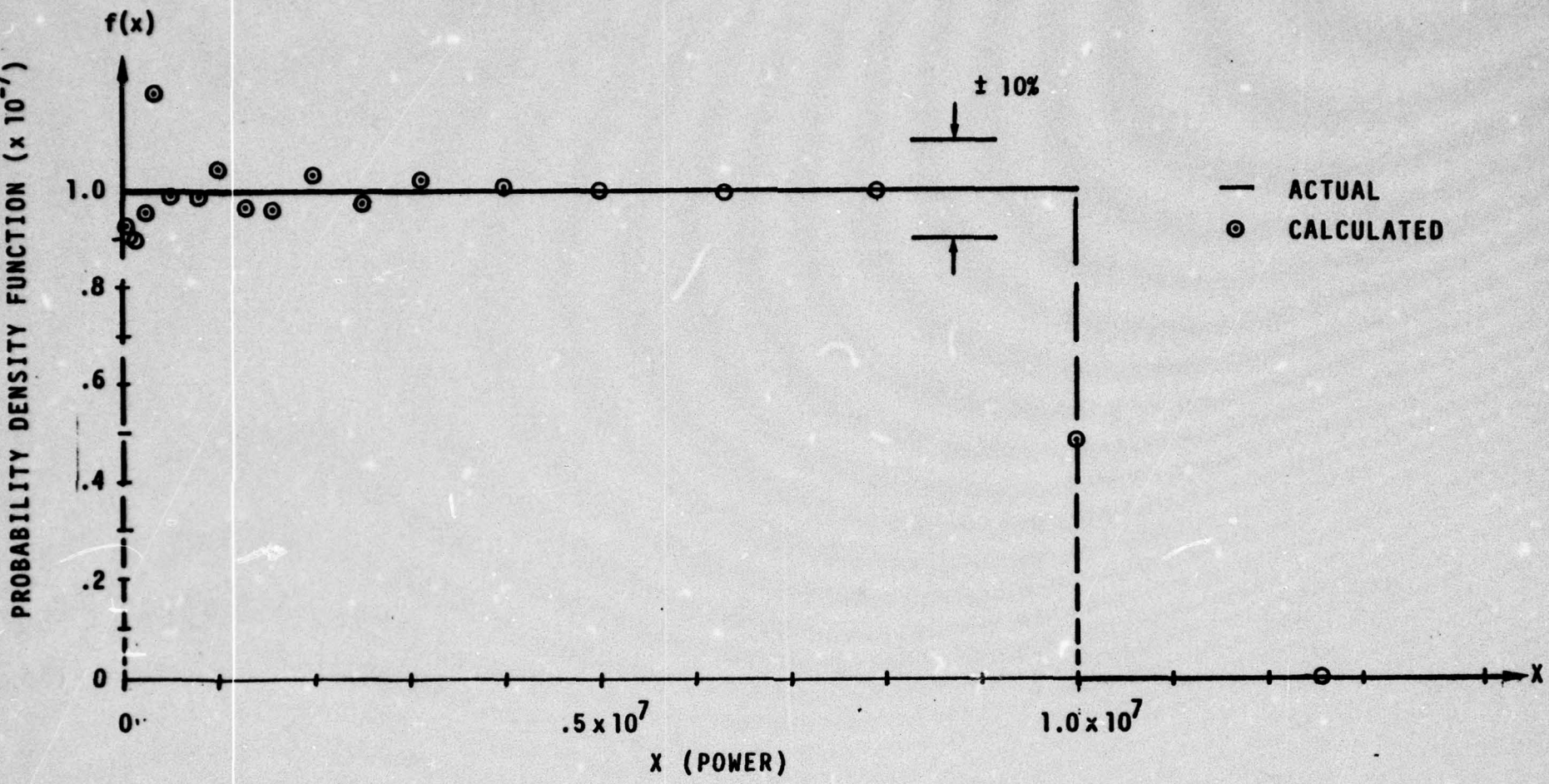

FIGURE 3.5 ACCURACY OF INVERSE FOURIER TRANSFORM ALGORITHM

Assume the joint characteristic function of two random variables is of the form:

$$\Phi_{XX\tau}(\alpha,\beta) = \Big(\zeta + R(\alpha,\beta)\Big) + j\ I(\alpha,\beta) \qquad (3\text{-}29)$$

where ζ is a constant, possibly zero, which is the multiplier of a unit impulse at the origin of the joint probability density space. Physically, ζ is the probability that the random variables X and X_τ both take on the value of zero.

Several properties of joint characteristic functions will be used to simplify the algorithm (Papoulis, op. cit.) The joint characteristic function obeys the inequality

$$|\Phi_{XX\tau}(\alpha,\beta)| \leq 1 \qquad (3\text{-}30)$$

for all α and β, with strict equality holding at $\alpha = 0$ and $\beta = 0$; i.e.,

$$\Phi_{XX\tau}(0,0) = 1\ . \qquad (3\text{-}31)$$

For $f_{XX\tau}$ a real function, the joint characteristic function has the symmetry properties

$$\Phi_{XX\tau}(-\alpha,-\beta) = \Phi^*_{XX\tau}(\alpha,\beta) \qquad (3\text{-}32)$$

and

$$\Phi_{XX\tau}(-\alpha,\beta) = \Phi^*_{XX\tau}(\alpha,-\beta) \qquad (3\text{-}33)$$

where * denotes complex conjugate. Substituting Equation (3-29) into Equation (3-3) and using the properties given above gives the joint probability density function as

$$f_{XX\tau}(x,x_\tau) = \zeta\delta(x,x_\tau)$$

$$+ \frac{1}{2\pi^2} \int_{-\infty}^{+\infty} \int_{0}^{+\infty} R(\alpha,\beta) \cos(\alpha x + \beta x_\tau)\, d\alpha\, d\beta$$

$$- \frac{1}{2\pi^2} \int_{-\infty}^{+\infty} \int_{0}^{+\infty} I(\alpha,\beta) \sin(\alpha x + \beta x_\tau)\, d\alpha\, d\beta \qquad (3\text{-}34)$$

since $f_{XX\tau}$ is real. Note that because of the symmetry properties in Equation 3-32, the integrals in Equation (3-34) have to be evaluated only over half of the α,β plane.

The values of $R(\alpha,\beta)$ and $I(\alpha,\beta)$ are assumed to have been computed at the sample points $\alpha(m)$ and $\beta(\ell)$, where $\alpha = 0$ or $\alpha(m) = +10^{m/40}$ for $m = -N, -N+1, \ldots, -1, 0$ and where $\beta = 0$ or $\beta(\ell) = \pm 10^{\ell/40}$ for $\ell = -N, -N+1, \ldots, -1, 0$.

Figure 3.6 shows representative sample points in the α,β plane. This scheme requires $2(N+1)^2 + 3(N+1)$ points for the real part and the same for the imaginary part.

The joint probability density function $f_{XX\tau}$ is computed at points $[x(n), x_\tau(p)]$ in the x, x_τ plane, where $x(n) = +10^{n/40}$ for $n = 0, 1, 2, \ldots, N$ and $x_\tau(p) = +10^{p/40}$ for $p = 0, 1, 2, \ldots, N$. Thus, $f_{XX\tau}$ will be computed at $(N+1)^2$ points.

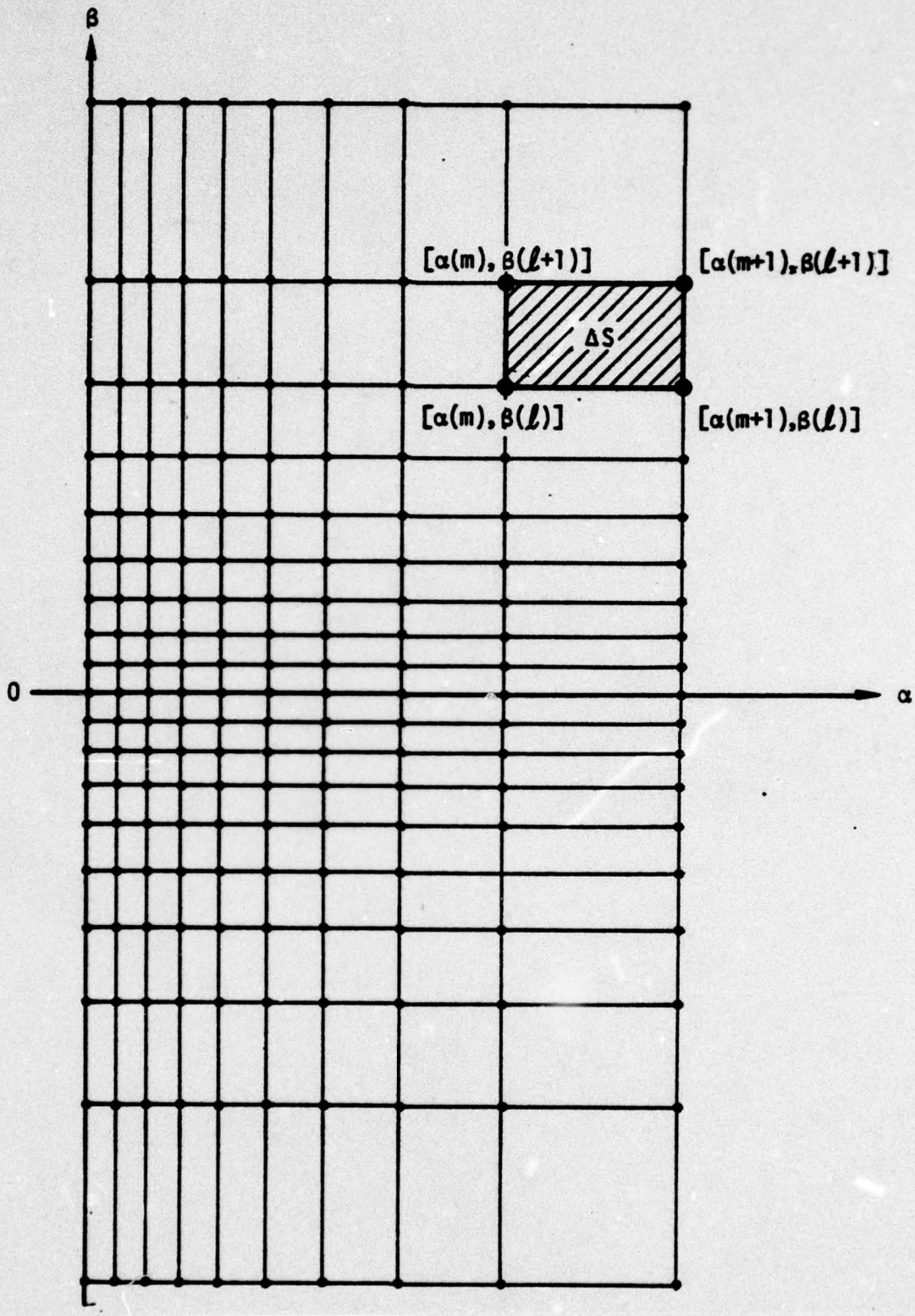

FIGURE 3.6 SAMPLE POINTS IN α,β PLANE SHOWING A GENERAL SEGMENT

If the integrals in Equation (3-33) are divided into segments, the formula for computing a given value of the joint probability density function becomes

$$f_{XX\tau}[x(n),\, x_\tau(p)] = \zeta\delta(x, x_\tau)$$

$$+ \frac{1}{2\pi^2} \sum_{\ell} \sum_{m} \int_{\beta(\ell)}^{\beta(\ell+1)} \int_{\alpha(m)}^{\alpha(m+1)} R(\alpha,\beta) \cos\left[\alpha x(n) + \beta x_\tau(p)\right] d\alpha\, d\beta$$

$$- \frac{1}{2\pi^2} \sum_{\ell} \sum_{m} \int_{\beta(\ell)}^{\beta(\ell+1)} \int_{\alpha(m)}^{\alpha(m+1)} I(\alpha,\beta) \sin\left[\alpha x(n) + \beta x_\tau(p)\right] d\alpha\, d\beta \qquad (3\text{-}35)$$

for n, p = 0, 1, 2, ..., N, where the summations are understood to be taken over the appropriate values of α and β. Figure (3-6) shows a general segment in the α,β plane.

An approximation is needed for $R(\alpha,\beta)$ and $I(\alpha,\beta)$ between sample points which achieves a balance between accuracy and realistic computer run times. The following scheme is felt to achieve this goal. Let $R(\alpha,\beta)$ and $I(\alpha,\beta)$ be approximated by a constant equal to the average value of the four corners of the segment. Therefore, for a general segment let the real part be approximated by the constant

$$R_{m\ell} = \frac{1}{4}\Big[R\left[\alpha(m),\, \beta(\ell)\right] + R\left[\alpha(m),\, \beta(\ell+1)\right] + R\left[\alpha(m+1),\, \beta(\ell)\right] + R\left[\alpha(m+1),\, \beta(\ell+1)\right]\Big] \qquad (3\text{-}36)$$

and the imaginary part by:

$$I_{m\ell} = \frac{1}{4}\Big[I[\alpha(m), \beta(\ell)] + I[\alpha(m), \beta(\ell+1)] + I[\alpha(m+1), \beta(\ell)] + I[\alpha(m+1), \beta(\ell+1)]\Big] \qquad (3\text{-}37)$$

for $\alpha(m) \leq \alpha \leq \alpha(m+1)$ and $\beta(\ell) \leq \beta \leq \beta(\ell+1)$ and zero otherwise.

Using the approximations given by Equations (3-36) and (3-37), the double integrals in Equation (3-35) can be evaluated and become

$$\int_{\beta(\ell)}^{\beta(\ell+1)} \int_{\alpha(m)}^{\alpha(m+1)} R_{m\ell} \cos[\alpha x(n) + \beta x_\tau(p)]\, d\alpha\, d\beta$$

$$= \frac{R_{m\ell}}{x(n)x_\tau(p)}\Big\{ \cos[\alpha(m)x(n) + \beta(\ell+1)x_\tau(p)] - \cos[\alpha(m)x(n) + \beta(\ell)x_\tau(p)] + \cos[\alpha(m+1)x(n) + \beta(\ell)x_\tau(p)] - \cos[\alpha(m+1)x(n) + \beta(\ell+1)x_\tau(p)] \Big\} \qquad (3\text{-}38)$$

and

$$\int_{\beta(\ell)}^{\beta(\ell+1)} \int_{\alpha(m)}^{\alpha(m+1)} I_{m\ell} \sin\ \alpha x(n) + \beta x_\tau(p)\ d\alpha\ d\beta$$

$$= \frac{I_{m\ell}}{x(n)x_\tau(p)} \Big\{ \sin\left[\alpha(m+1)x(n) + \beta(\ell+1)x_\tau(p)\right]$$

$$- \sin\left[\alpha(m+1)x(n) + \beta(\ell)x_\tau(p)\right]$$

$$+ \sin\left[\alpha(m)x(n) + \beta(\ell+1)x_\tau(p)\right]$$

$$- \sin\left[\alpha(m)x(n) + \beta(\ell)x_\tau(p)\right]\Big\} \qquad (3\text{-}39)$$

By substituting Equations (3-36) through (3-39) into Equation (3-35), using trigonometric identities for the cosine and sine of sums, and appropriately evaluating the sums, we find that the algorithm for computing the joint probability density function can be put into the form

$$f_{XX\tau}[x(n),x_\tau(p)] \simeq \zeta\delta(x,x_\tau)$$

$$+ \frac{1}{2\pi^2 x(n)x_\tau(p)} \sum_{\ell} \Big\{ \left[\sin \beta(\ell+1)x_\tau(p)\right.$$

$$\left. - \sin \beta(\ell)x_\tau(p)\right]$$

$$\times \sum_{m} \Big[R_{m\ell} \left[\sin \alpha(m+1)x(n) - \sin \alpha(m)x(n)\right]$$

$$- I_{m\ell} \left[\cos \alpha(m+1)x(n) - \cos \alpha(m)x(n)\right] \Big]$$

..... continued to next page

$$+ [\cos \beta(\ell) x_\tau(p) - \cos \beta(\ell+1) x_\tau(p)]$$

$$+ \sum_m \Big\{ R_{m\ell} [\cos \alpha(m+1)x(n) - \cos \alpha(m)x(n)]$$

$$+ I_{m\ell} [\sin \alpha(m+1)x(n) - \sin \alpha(m)x(n)] \Big\} \qquad (3\text{-}40)$$

for n, p = 0, 1, 2, ..., N. Note in Equation (3-40) that the summations over ℓ and m must be taken with the appropriate data points, including when $\alpha = 0$ or $\beta = 0$ and when $\beta(\ell)$ is negative.

4.0 CHARACTERISTIC FUNCTIONS FOR SOURCES

4.1 Introduction

The calculation of the joint characteristic function for the averaged squared noise pressure X at a point, and its value X_τ at τ time units later requires a source characteristic function for each type of ship. The specific quantity required is the characteristic function for the averaged squared pressure of the noise radiated by the ship in a specified 1-Hz band referred to a unit distance from the acoustic center.

Heine and Gray* have derived a source level model for merchant ships. The model consists of the expected distributions in both source pressure level and frequency of four significant acoustic signature components for the world's merchant fleet of cargo, passenger, and fishing vessels.

The signature components that were characterized are (1) the broadband component related to the collapse of propeller cavitation bubbles; (2) narrowband components at the propeller blade rate and its harmonics which are related to the modulation of the cavitation by the spatially varying inflow to the propeller; (3) narrowband components at the diesel firing rate and its harmonics which are related to the vibratory forces of the main propulsion diesel engine; and (4), the narrowband component at the ship's electric plant frequency.

---

*J. C. Heine, L. M. Gray, "Merchant Ship Radiated Noise Model," Bolt Beranek and Newman Inc. Report No. 3020, August 1976.

Explicit expressions relating the source levels and frequencies of each component to the engineering parameters of the noise-producing mechanisms were derived. These expressions were used to estimate the distributions of source levels of each component for the ensemble of merchant ships at sea, based on a survey of the distributions of the engineering parameters within the earth's merchant fleet.

Based on consideration of significant differences in the distributions of peak levels and associated frequencies of the continuous cavitation spectrum, all merchant vessels can be considered to be in one of eight broadband classes, each with its own characteristic spectrum.

Consideration of significant differences in the mean values of the distributions of levels and center frequencies of the fundamental of each narrowband component led to the definition of three narrowband classes, independent of the broadband classes: (1) fishing vessels; (2) merchant ships over 500 gross (long) tons and less than 700 feet long; and (3) merchant vessels over 700 feet long.

The method for utilizing the predictions of Heine and Gray consists of finding the source characteristic functions for each component of a class signature, and then calculating their product to obtain the composite characteristic function. Section 4.2 details the procedure for the narrowband sources, and 4.3 deals with the broadband component. Finally, Section 4.4 applies the method to a case of a 1-Hz band centered at 100 Hz.

4.2 Narrowband Sources

The method discussed in Section 4.1 for deriving the source characteristic functions for various classes of ships requires the characteristic functions for the various narrowband sources associated with these classes of ships. The required characteristic functions for narrowband sources were obtained by means of a three-step process: (1) obtain the probability density function for source pressure level; (2) transform that result to the probability density function of the averaged squared pressure at one yard; and (3) transform that result to the characteristic function of the averaged squared pressure at one yard.

The first step of the process, obtaining the probability density function for the narrowband source level, is based on the data of BBN Report No. 3020 as represented in Figure 4.1, which gives histograms for both the source pressure level and the frequency of the fundamental component. Let Y be the source pressure level in a specified 1-Hz band from a particular narrowband source that radiates harmonics as well as the fundamental. If the fundamental is greater than 1 Hz, then no more than one component of the harmonic set can fall in a 1-Hz increment of frequency. Let

A_0 be the event that no component falls in the designated 1-Hz band

A_1 be the event that the fundamental falls in the designated 1-Hz band

A_2 be the event that the first harmonic falls in the designated 1-Hz band, and so on

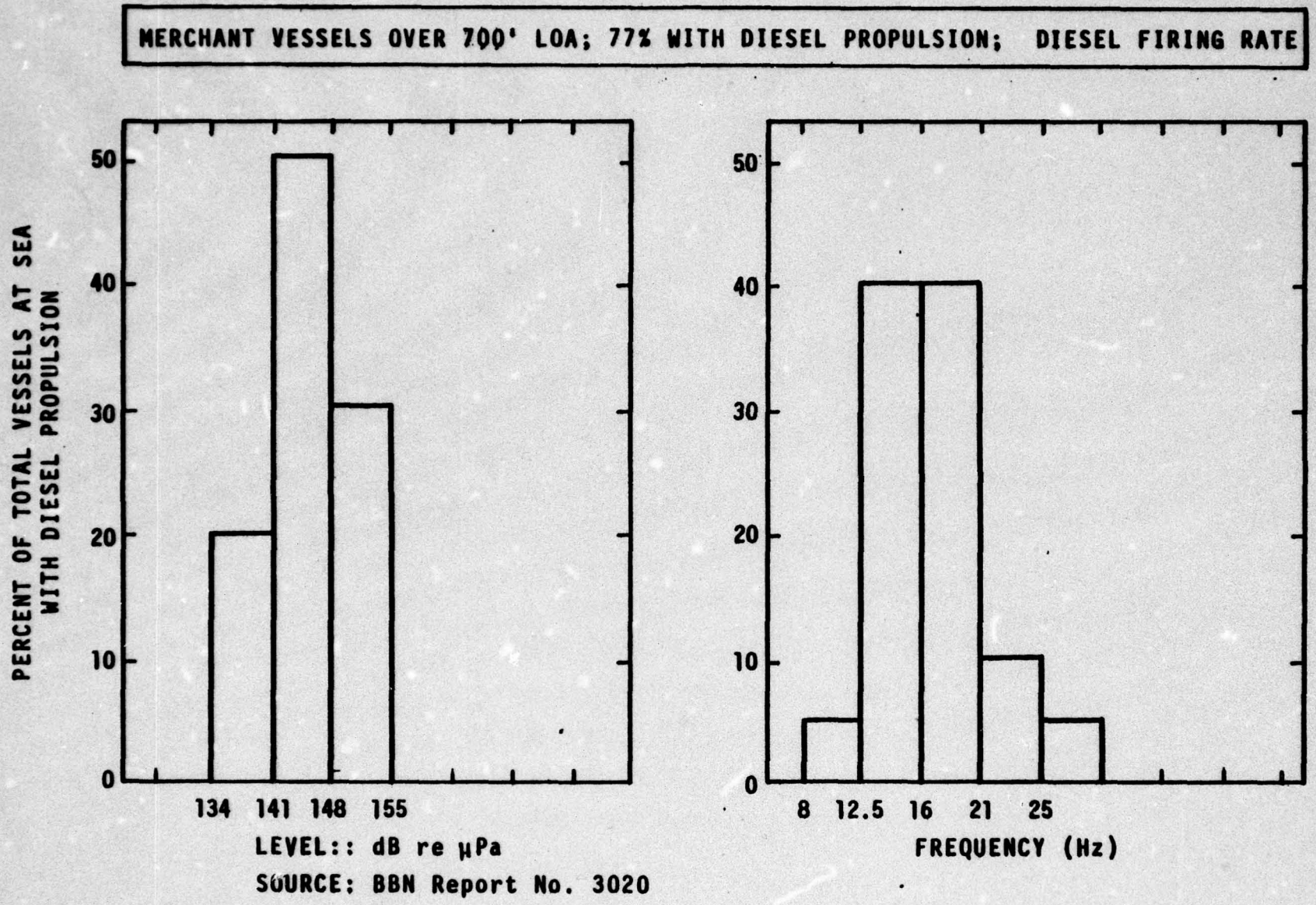

FIGURE 4.1 NARROWBAND PROBABILITY DISTRIBUTION: LARGE MERCHANT VESSELS, DIESEL FIRING RATE

With the stipulation that the frequency of the fundamental is greater than 1 Hz, these events are mutually exclusive; that is, only one of the events can occur in a single performance of the experiment.

According to the total probability theorem for mutually exclusive events, the probability distribution function for Y is

$$F_Y(y) = \sum_{i=0}^{\infty} P(Y \leq y | A_i) P(A_i). \qquad (4\text{-}1)$$

The corresponding probability density function is

$$f_Y(y) = \frac{d}{dy} F_Y(y)$$

$$= \sum_{i=0}^{n} f_Y(y|A_i) P(A_i) \qquad (4\text{-}2)$$

A histogram such as that shown on the left side of Figure 4.1 can be used to obtain the conditional probability density functions for the fundamental source pressure level. In this example, the total area under the bars is 700 (dB x %); thus, $f_Y(y|A_1)$ is obtained by dividing the ordinates of the histograms by 700. That result in turn can be used to get the conditional probability density function for a harmonic source pressure level by shifting the curve to the left by the number of dB that the harmonic level is below that of the fundamental.

A histogram such as that shown on the right side of Figure 4.1 can be used to obtain the probability that the fundamental component falls in a specified 1-Hz band. For

example, suppose that the 1-Hz band is centered on 20 Hz. The histogram shows that there is a 40% chance that the fundamental frequency is in the 5-Hz interval between 16 and 21 Hz. Thus,

$$P(A_1) = \frac{40\%}{100\%} \cdot \frac{1\ \text{Hz}}{5\ \text{Hz}} = 0.08 \qquad (4\text{-}3)$$

For the first harmonic, the numbers on the frequency scale of the sample histogram would be doubled. Thus, there is a 5% chance that the second harmonic falls in the 9-Hz frequency band between 2 x 8 = 16 and 2 x 12.5 = 25 Hz. Thus,

$$P(A_2) = \frac{5\%}{100\%} \times \frac{1\ \text{Hz}}{9\ \text{Hz}} = 0.0055 \qquad (4\text{-}4)$$

For this example, it is seen that the probability that the second harmonic falls in the 1-Hz band centered at 20 Hz is zero. The probability that no harmonic falls in the designated 1-Hz band is

$$P(A_0) = 1 - P(A_1) - P(A_2) - \ldots \qquad (4\text{-}5)$$

For the example being considered, $P(A_0) = 0.9145$. Finally, the conditional density function for the event A_o is

$$f_Y(y|A_0) = \delta[y - (-\infty)] \qquad (4\text{-}6)$$

where $\delta(\ )$ is the unit delta function. An alternative to (4-2) that makes the delta function explicit is

$$f_Y(y) = P(A_0)\delta(y + \infty) + g_Y(y) \qquad (4\text{-}7)$$

where

$$g_Y(y) = \sum_{i=1}^{\infty} f_Y(y|A_i)P(A_i) \qquad (4\text{-}8)$$

Since the source pressure level is $Y = 10 \log_{10} W$, then

$$f_W(w) = P(A_0)\delta(w) + 4.34w^{-1} g_Y(10 \log_{10} w) \qquad (4\text{-}9)$$

and the corresponding characteristic function is

$$\Phi_W(\omega) = \int_{\infty}^{\infty} \exp(j\omega w) f_W(w) dw \qquad (4\text{-}10)$$

4.3 Broadband Component

The broadband component of the radiated noise is related to the collapse of propeller cavitation bubbles. From a consideration of significant differences in the distributions of peak levels and associated frequencies of the continuous cavitation spectrum, all merchant vessels were distributed among eight broadband classes (Heine and Gray, op. cit.), each with its characteristic spectrum as shown in Figure 4.2.

The distribution of these broadband classes among small (over 500 gross long tons and less than 700 feet) and large (over 700 feet) merchant ships is shown by Figures 4.3 and 4.4 respectively. These data, along with those of Figure 4.2, provide a basis for deriving the probability density function for the broadband source levels for small and large merchant ships.

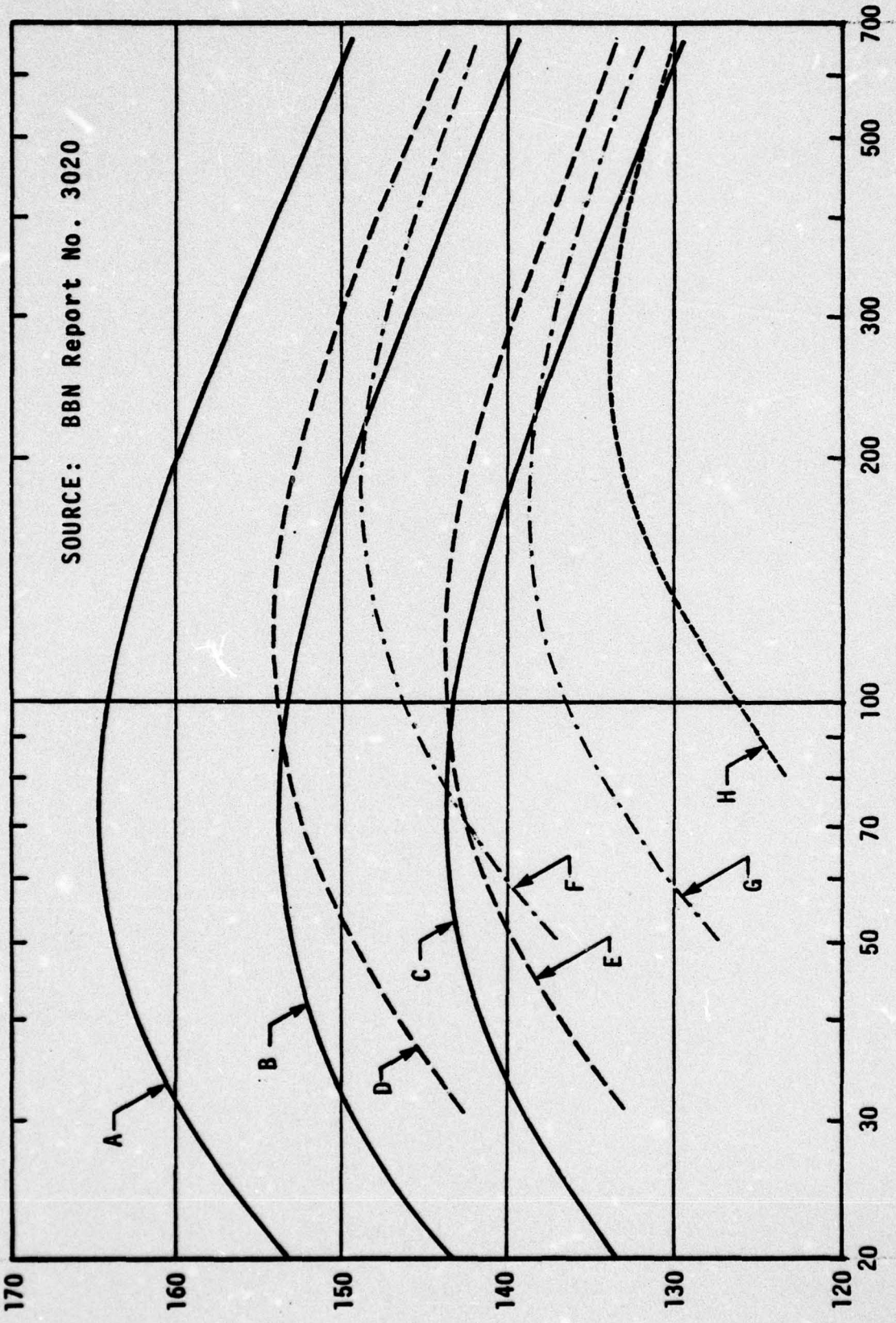

FIGURE 4.2 BROADBAND ACOUSTIC CLASS SPECTRA

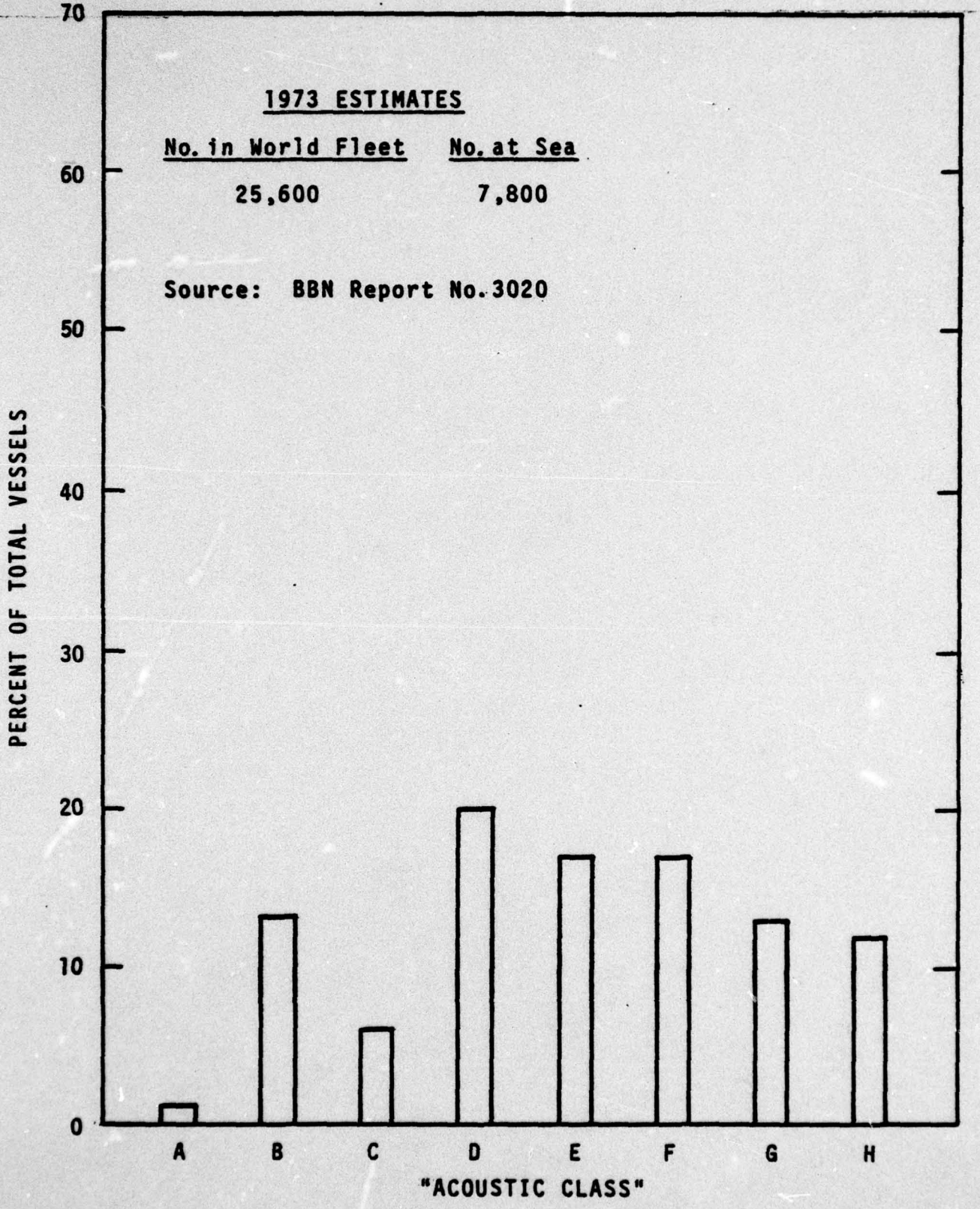

FIGURE 4.3 DISTRIBUTION OF BROADBAND CLASSES, MERCHANT VESSELS LESS THAN 700 FT. LOA

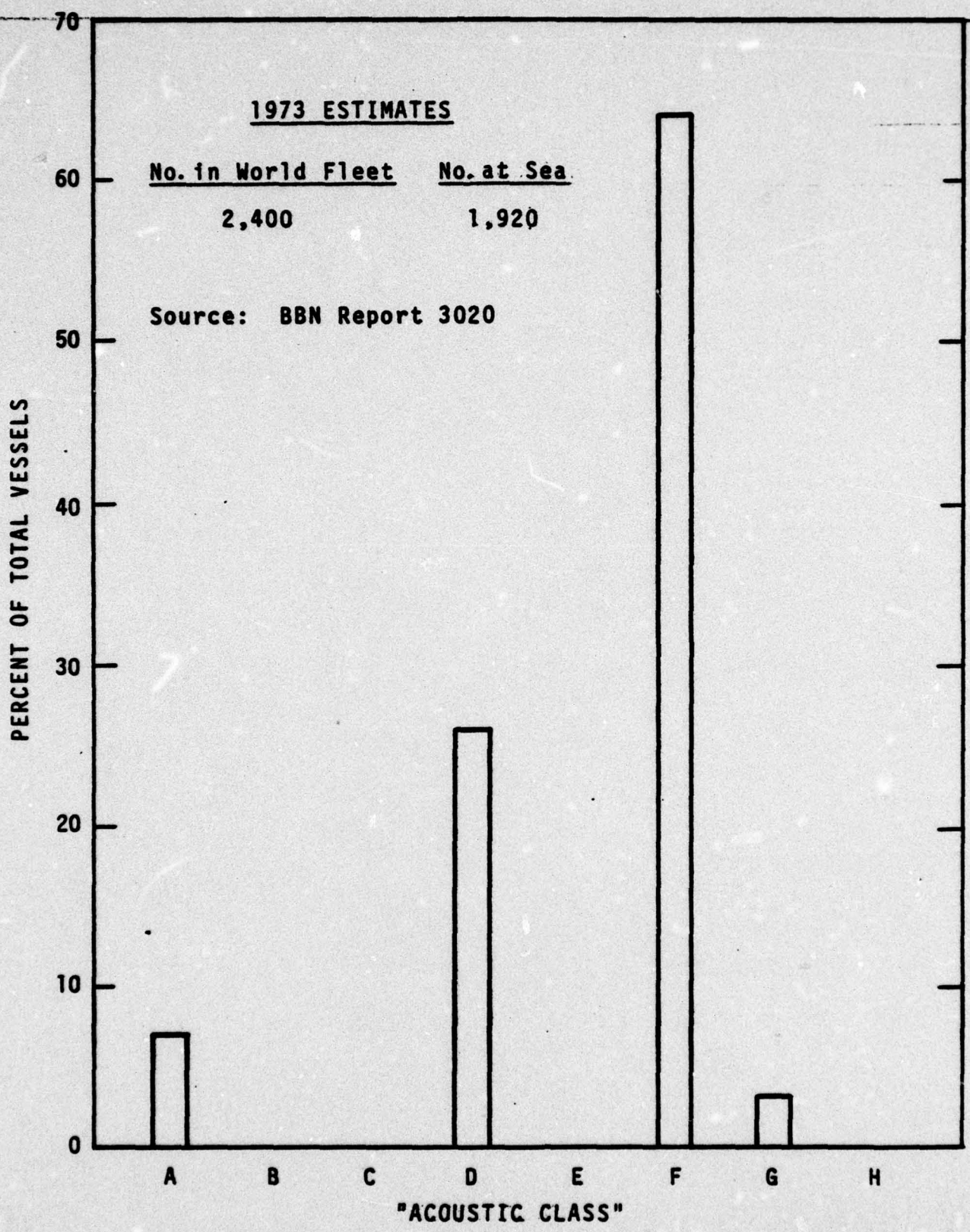

FIGURE 4.4 DISTRIBUTION OF BROADBAND CLASSES, MERCHANT VESSELS GREATER THAN 700 FT. LOA

First, for a given frequency of interest, the source spectrum level for each broadband class is obtained from Figure 4.2. Second, the probability of occurrence of the broadband class for each type of merchant ship is determined from Figures 4.3 and 4.4. These data were employed to construct discrete probability distribution of source levels for each type of ship. Finally, these discrete probabilities were distributed over 10 dB increments of source level to obtain probability density functions for broadband source spectrum levels.

4.4 Results of Calculations

The methods for obtaining the broadband and narrowband components of radiated noise discussed in the previous sections were applied to a case of a 1-Hz band centered at 100 Hz.

Figures 4.5, 4.6 and 4.7 show the resulting probability density function of the source level of the diesel firing rate, blade rate and broadband components, respectively, for merchant ships less than 700 feet LOA. For the narrowband sources, there is a high probability that there is no energy in the selected band, as indicated by the values given for $P(-\infty)$. Figures 4.8, 4.9 and 4.10 show the resulting probability density function of source level of the diesel firing rate, blade rate and broadband components, respectively, for merchant ships greater than 700 feet. No electric plant lines are assumed present at 100 Hz.

Each of the three noise sources (diesel firing rate, blade rate and broadband) is considered to be an independent random variable. The random variable of the mean square pressure

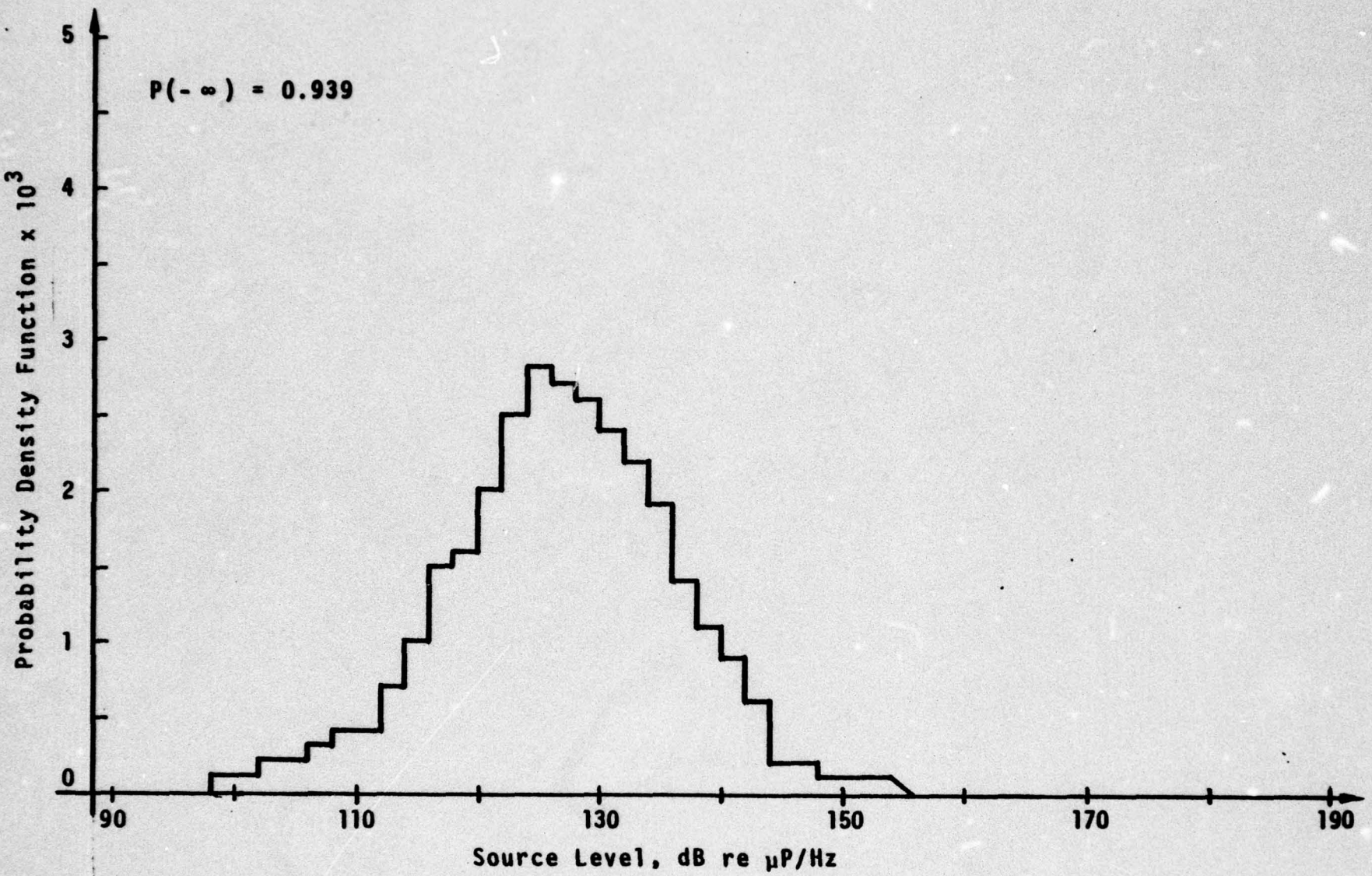

FIGURE 4.5 DIESEL FIRING RATE DENSITY FUNCTION FOR MERCHANT SHIPS LESS THAN 700 FT. (FREQ = 100 HZ)

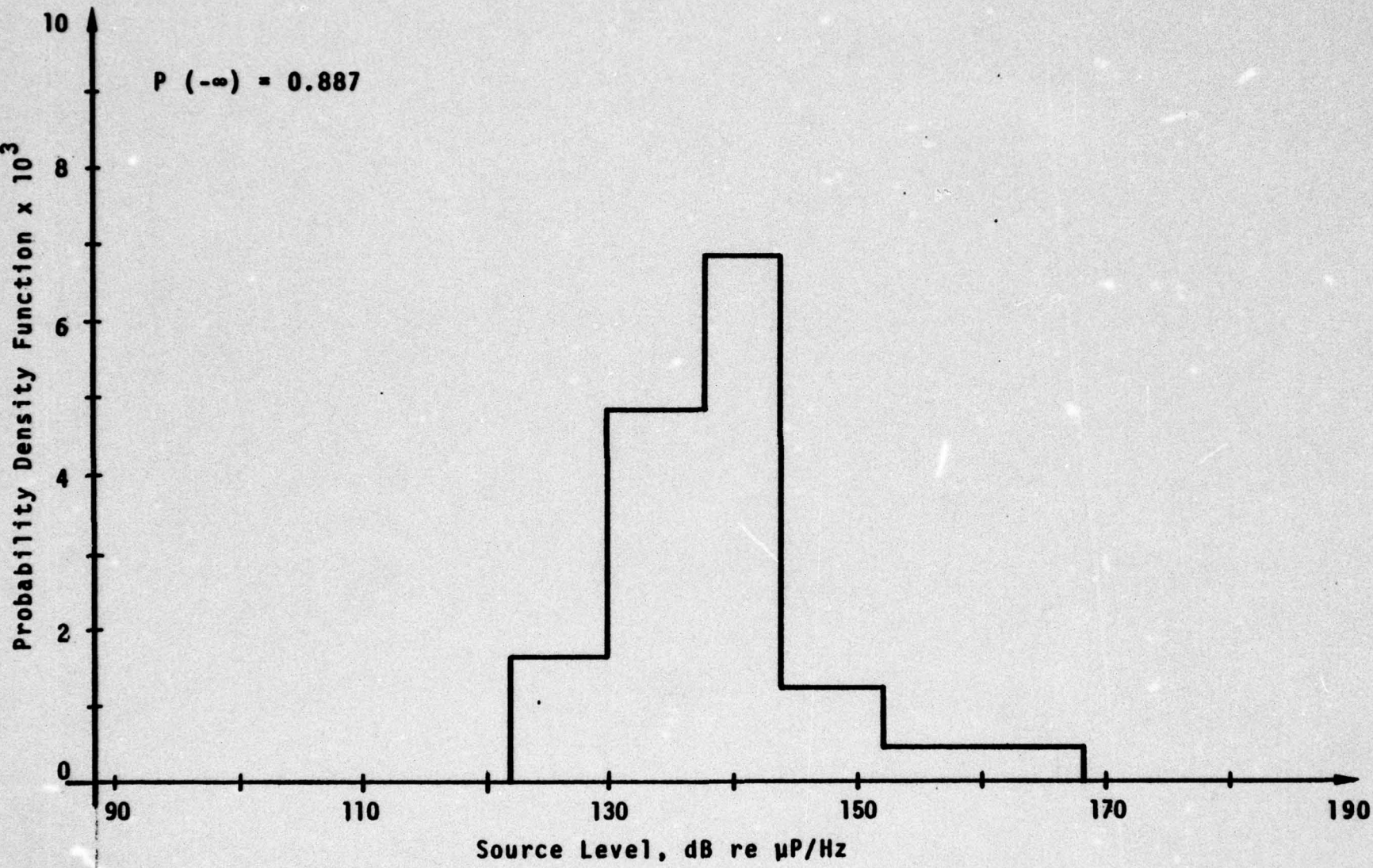

FIGURE 4.6 BLADE RATE DENSITY FUNCTION FOR MERCHANT SHIPS LESS THAN 700 FT.
[FREQ = 100 HZ]

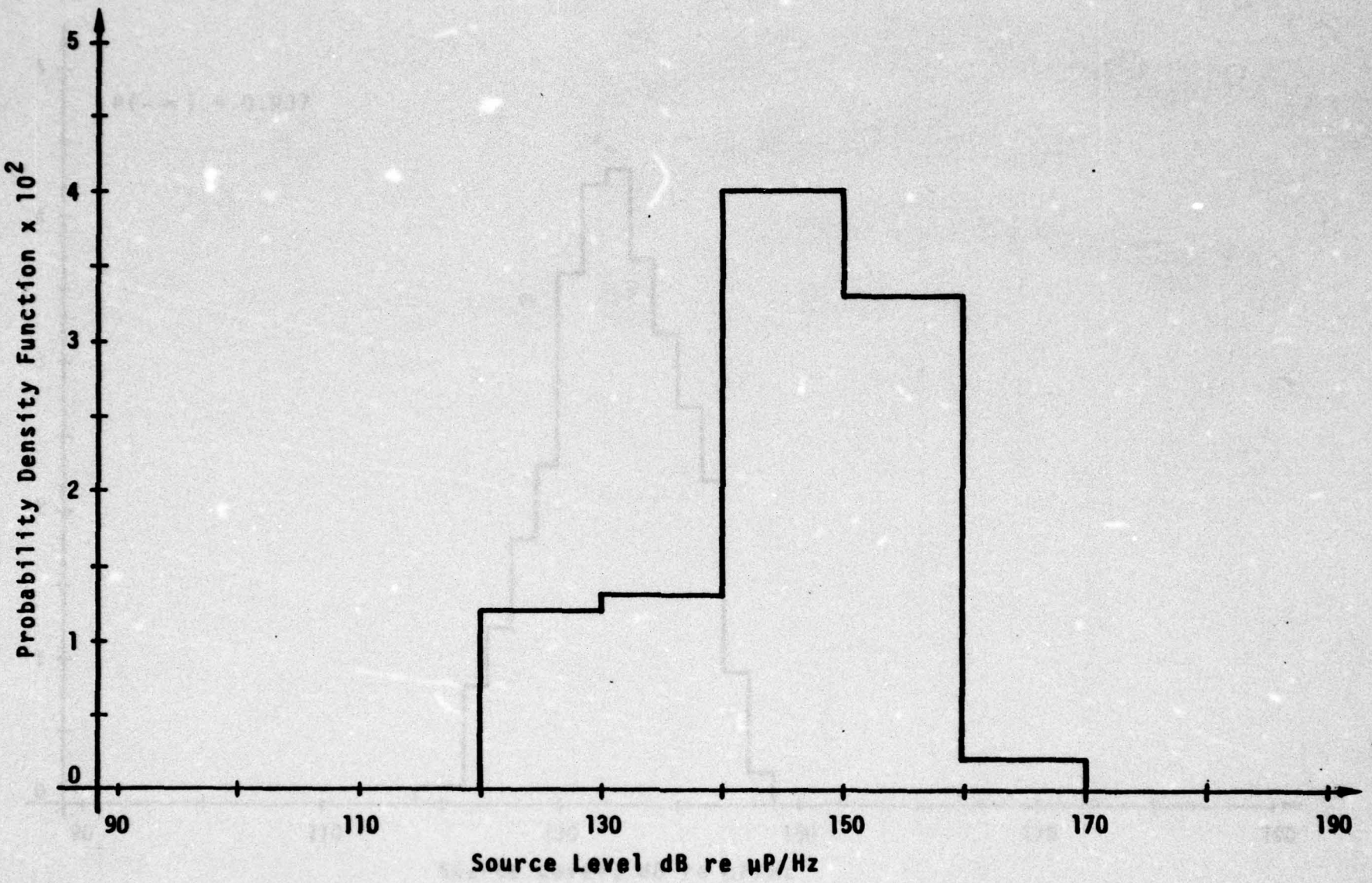

FIGURE 4.7 BROADBAND DENSITY FUNCTION FOR MERCHANT SHIPS LESS THAN 700 FT. (FREQ = 100 HZ)

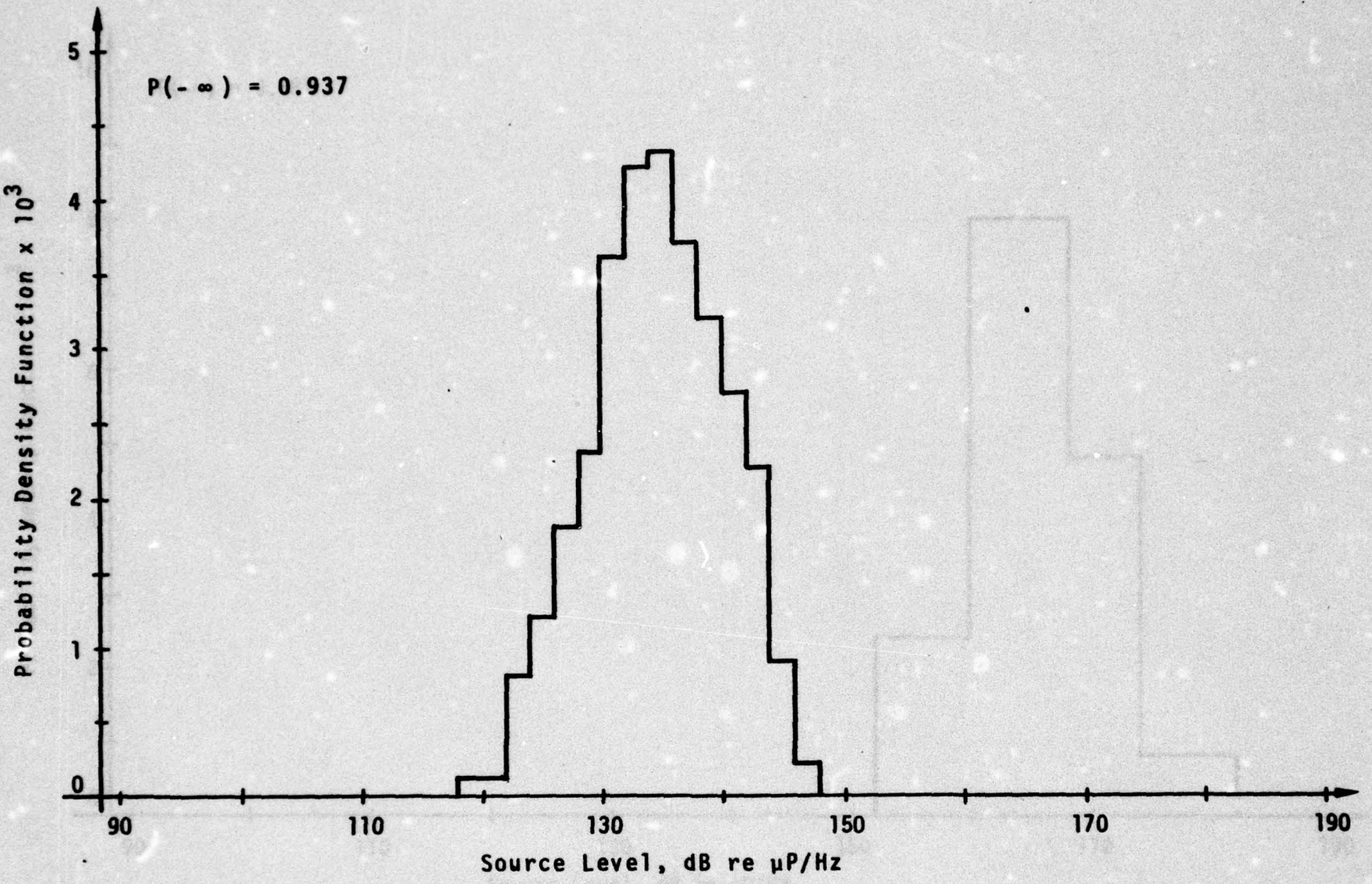

FIGURE 4.8 DIESEL FIRING RATE DENSITY FUNCTION FOR MERCHANT SHIPS GREATER THAN 700 FT. [FREQ = 100 HZ]

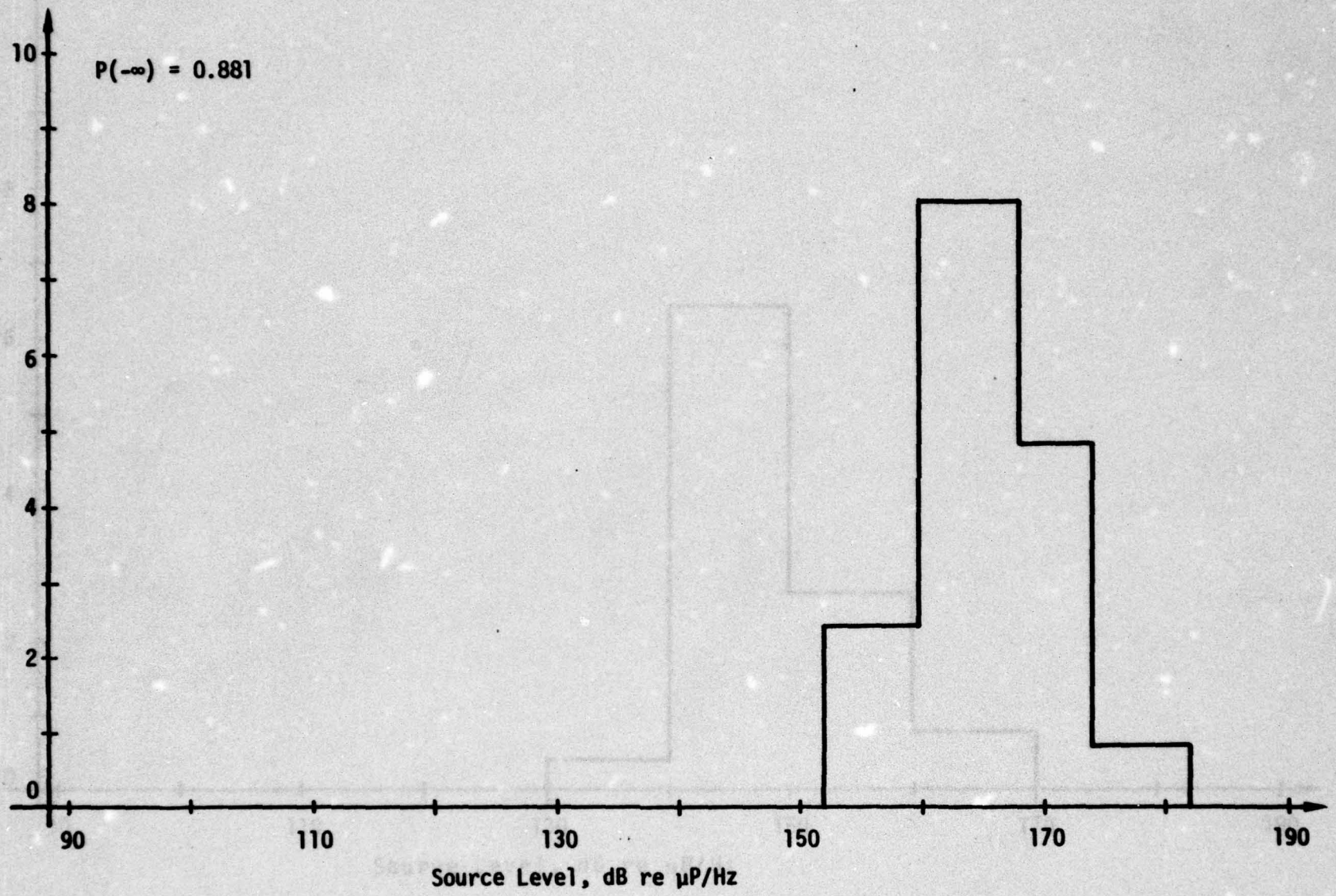

FIGURE 4.9 BLADE RATE DENSITY FUNCTION FOR MERCHANT SHIPS GREATER THAN 700 FT. [FREQ = 100 HZ]

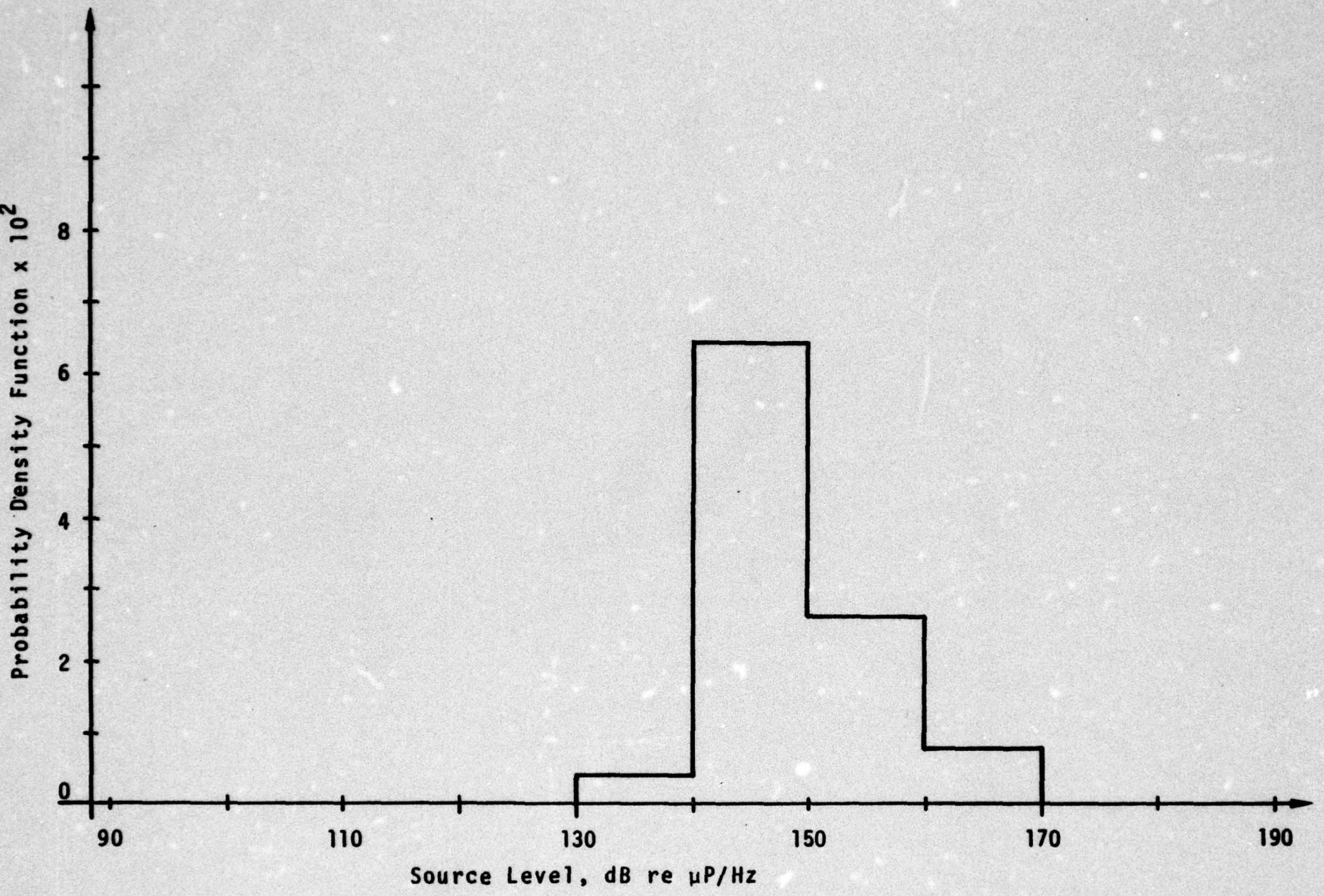

FIGURE 4.10 BROADBAND DENSITY FUNCTION FOR MERCHANT SHIPS GREATER THAN 700 FT.
[FREQ = 100 HZ]

of the total radiated noise is the sum of these three components. Therefore, the probability density function of the total radiated noise is equal to the convolution of the densities of the random variables in the sum. A computationally convenient method of performing the convolution is to transform the density functions to characteristic functions and to multiply them.

Figure 4.11 shows a block diagram of the program used to compute the characteristic function of total radiated noise for each type of merchant ship. The inputs to the program were the densities shown in Figures 4.5 through 4.10. One of the outputs from the program was used as the input to the program which computes the probability density of the mean square pressure of the received noise (i.e., described in Section 5). The Fourier transform algorithm used was that described in Section 3.

Figure 4.12 shows the density function for the total radiated noise level for merchant ships less than 700 feet. Figure 4.13 shows the results for merchant ships greater than 700 feet. In each figure, a curve has been fitted to the actual computed data. Table 4.1 gives the mean value, variance and standard deviation in power for the total radiated noise for each type of merchant ship.

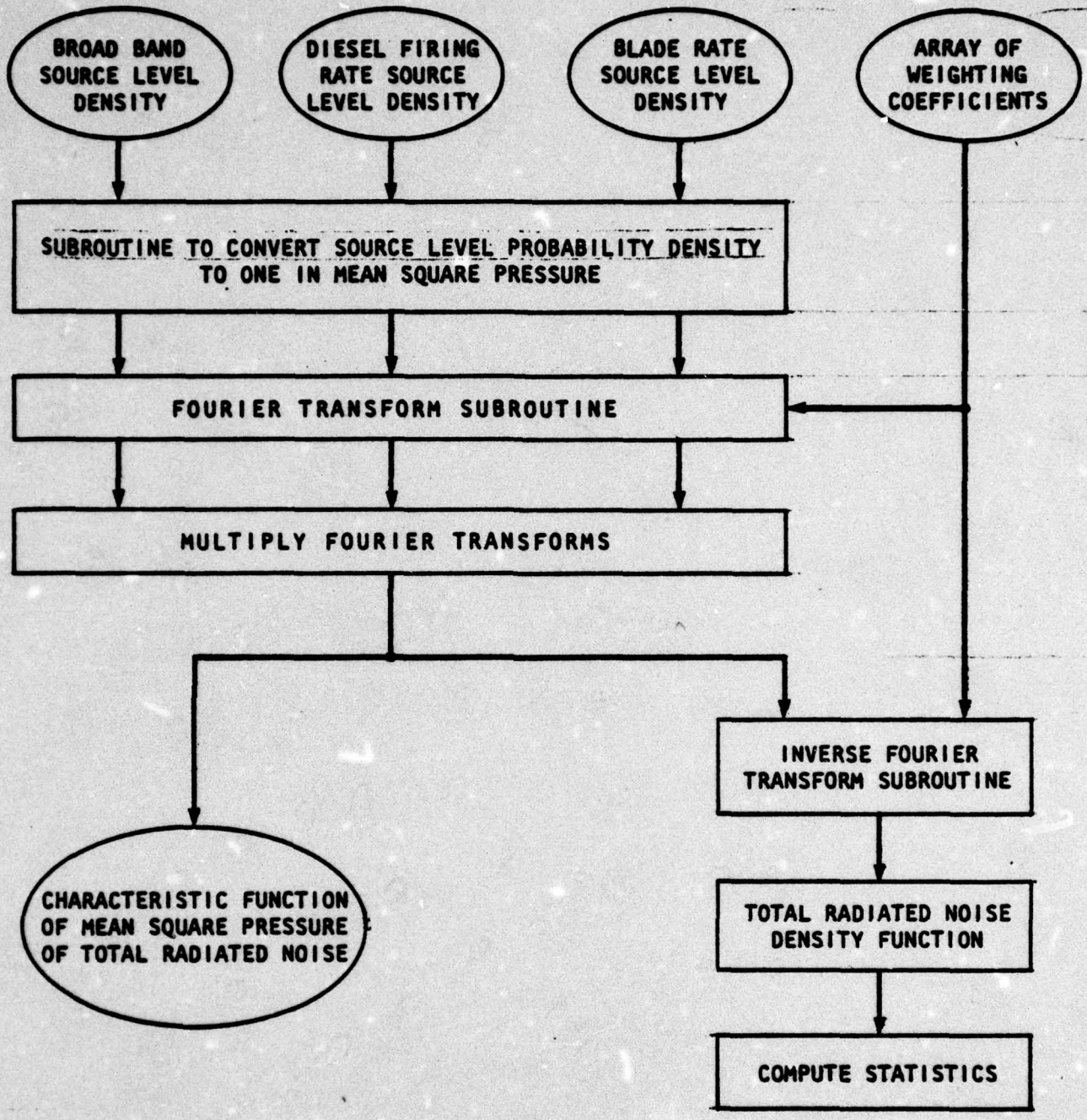

FIGURE 4.11 BLOCK DIAGRAM OF TOTAL RADIATED NOISE COMPUTER PROGRAM.

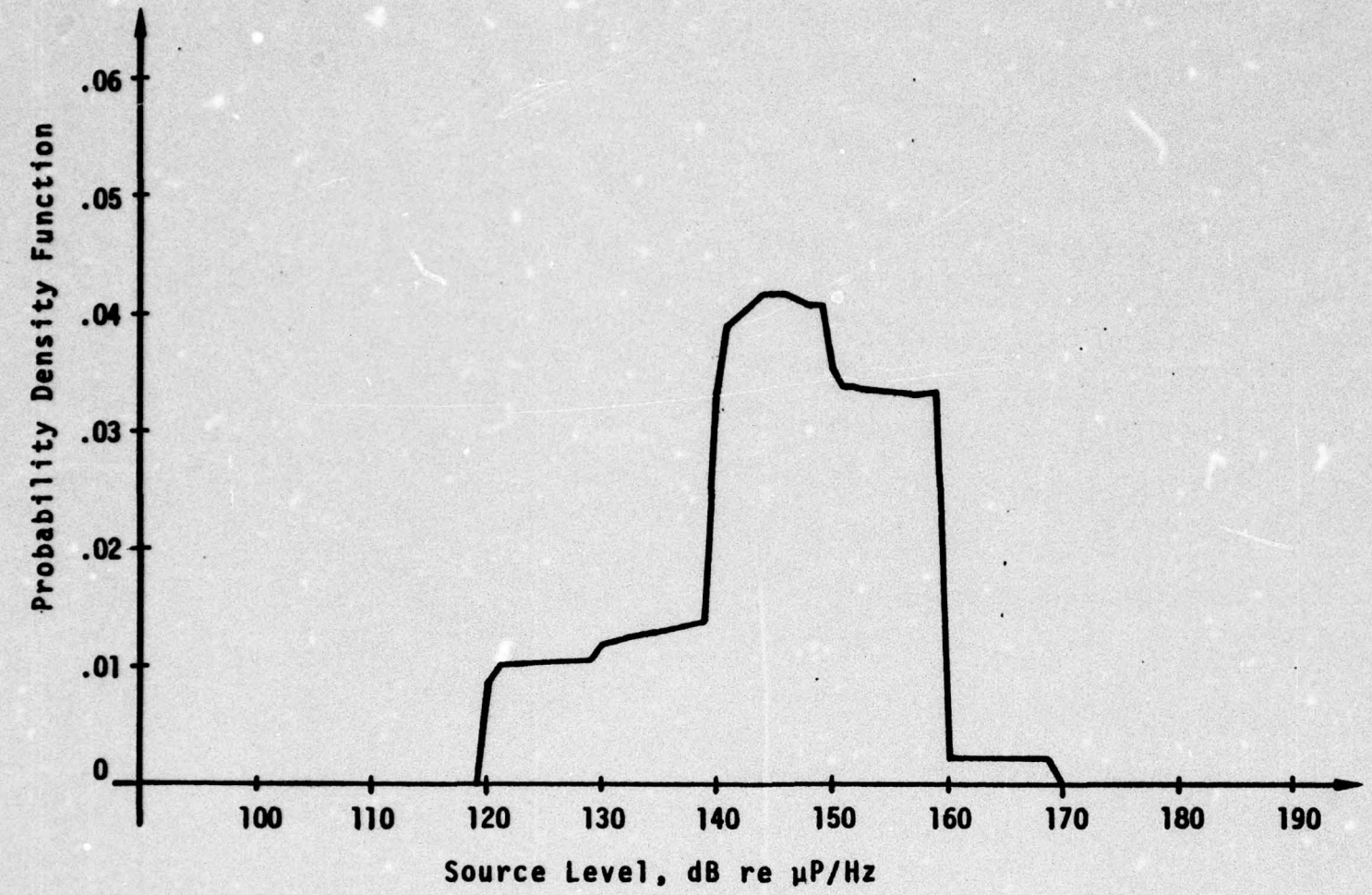

FIGURE 4.12 TOTAL RADIATED NOISE PROBABILITY DENSITY FUNCTION OF SOURCE LEVEL FOR MERCHANT SHIPS LESS THAN 700 FT. LOA [FREQ = 100 HZ]

FIGURE 4.13 TOTAL RADIATED NOISE PROBABILITY DENSITY FUNCTION OF SOURCE LEVEL FOR MERCHANT SHIPS GREATER THAN 700 FT. LOA (FREQ = 100 HZ)

Table 4.1 Moments of Total Radiated Noise Density for 1-Hz Band at 100 Hz

	Mean Value of Mean Square Pressure, $(\mu P)^2$	Variance of Mean Square Pressure, $(\mu P)^4$	Standard Deviation of Mean Square Pressure, $(\mu P)^2$
Merchant Vessels Less Than 700 ft. LOA	2.36×10^{15}	4.88×10^{31}	6.99×10^{15}
Merchant Vessels Greater Than 700 ft. LOA	1.61×10^{16}	6.14×10^{33}	7.84×10^{16}

5.0 DESCRIPTION OF COMPUTER PROGRAM

The digital computer program that has been implemented for the prediction of averaged squared pressure of ambient noise due to merchant shipping is described in this section. Figure 5.1 presents a block diagram for this program.

The inputs to the program are the sensor information, the route information, characteristic functions of ship radiated noise, a transmission loss function, and an array of weighting coefficients for the inverse Fourier transform algorithm. The sensor information consists of the latitude and longitude of the sensor, the true bearing of the center of the observation sector, and the width of the sector. For each route crossing the sector, the route information consists of the latitude and longitude of the point of departure, nominal course, transverse route width, and ship traffic density.

The characteristic functions of ship radiated noise for each type of ship is read from a disk file. The calculation of the source characteristic functions is described in Section 4.

The transmission loss function to be used in the computations is stored on a disk file as a table of transmission loss versus range. This table is read by the program as an input.

The array of weighting coefficients that is used by the inverse Fourier transform algorithm must be pre-computed and stored on a disk file. These weighting coefficients, discussed in Section 3, are read by the program as an input.

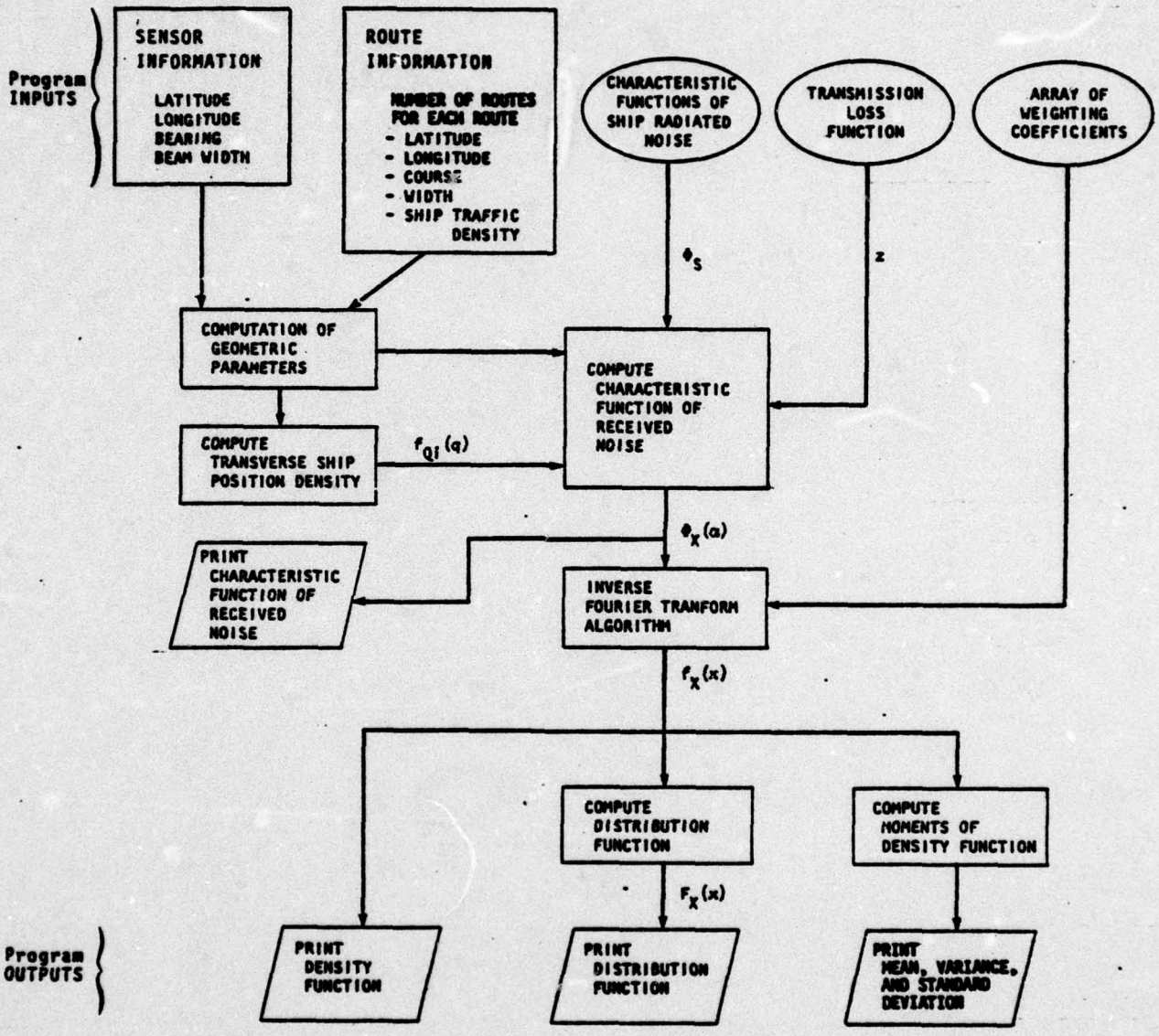

FIGURE 5.1 COMPUTER PROGRAM BLOCK DIAGRAM

The main portion of the computer program consists of code to compute the characteristic function of received noise, $\Phi_X(\alpha)$. The defining formulas and relevent discussion are found in Section 2. The main portion of the computer program makes use of other subsections of code, in the form of subroutines.

One of these subroutines computes the geometric parameters from the sensor and route information. The geometry considerations are also discussed in Section 2. Another of these subroutines computes the transverse ship position density $f_{Qi}(q)$ from the route width and geometric parameters. The characteristic function $\Phi_X(\alpha)$ can be printed if desired.

Next in the program the characteristic function $\Phi_X(\alpha)$ and the arrays of weighting coefficients are used as input to the inverse Fourier transform algorithm. This algorithm, described in Section 3, computes the probability density function of received noise $f_X(x)$. Once the density function has been computed, another section of code computes the moments of the density function and computes the probability distribution function $F_X(x)$.

The final section of the computer program prints out the density function, distribution function, the mean, variance and the standard deviation of the mean square pressure of the received noise.

6.0 EXAMPLES

This section presents some examples of the use of the Ambient Noise Model. Three different examples were run to demonstrate and check the model. The first example shows the effects of various ship traffic densities. The second shows the effects of range. The last example shows the effects of changes in the route width. For all of the examples presented in this section, the transmission loss model was

$$TL = 48 + 20 \log R + 2.025 \alpha R, \qquad (6\text{-}1)$$

$$\text{for } R \leq 243.5 \text{ n.m.}$$

$$TL = 72 + 10 \log R + 2.025 \alpha R, \qquad (6\text{-}2)$$

$$\text{for } R \geq 243.5 \text{ n.m.}$$

where TL = transmission loss in dB,
R = range in nautical miles, and
$\alpha = 10^{-3}$ for f = 100 Hz.

This was an input to the computer program as described in Section 5. The transmission loss was input in the form of a table of transmission loss in power versus range, for one nautical mile increments from 1 to 1,000 n.m.

The transverse ship position density $f_{Q1}(q)$ used in the program was the Beta density function centered on the nominal course and zero outside the route width.

The ship source model used in all the examples of this section are those characteristic functions of the total radiated noise density functions for small merchant ships and for large merchant ships, for a 1-Hz band centered at 100 Hz, as described in Section 4.4.

6.1 Example 1 — Various Ship Traffic Densities

The route and sensor geometry for this example are shown in Fig. 6.1. The sensor had a beam width of 5 degrees. The received noise was for a one-Hertz band centered at 100 Hertz. The range to the intersection of the center of the beam and center of the route was 541.5 n.m. The single route had a width of 30.0 n.m.

Three cases of ship traffic density were processed. They were:

	Large Ships	Small Ships
Case 1	0.025/n.m.	0.025/n.m.
Case 2	0.050/n.m.	0.050/n.m.
Case 3	0.100/n.m.	0.100/n.m.

Figure 6.2 shows, for the three cases, probability density functions of the noise as received at the sensor from the sector. Figure 6.3 shows the corresponding probability distribution functions plotted on probability paper. In both figures smooth curves have been fitted to the actual data printed out by the computer. Table 6.1 gives some of the statistical measures of the received noise.

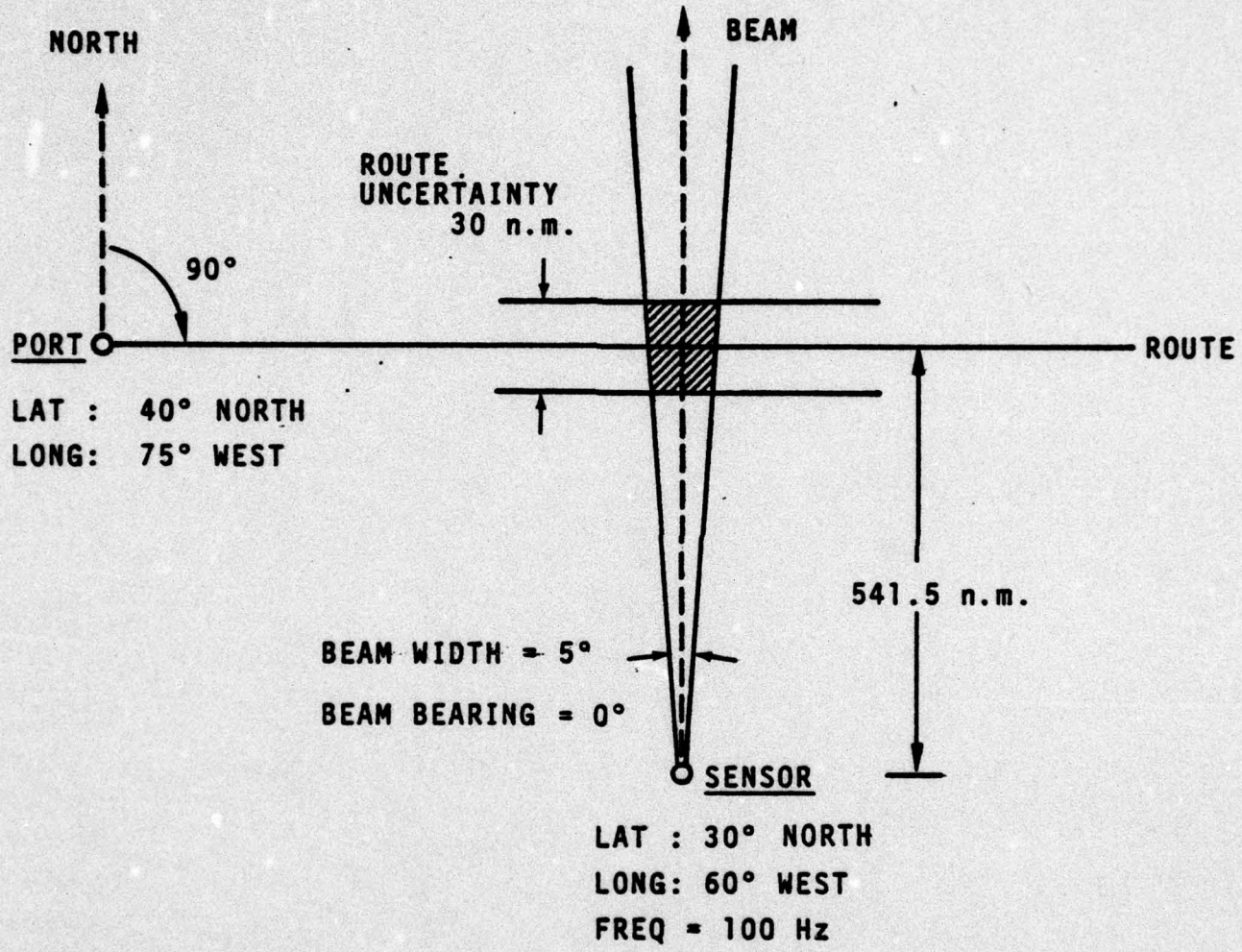

FIGURE 6.1 ROUTE AND SENSOR GEOMETRY FOR THE EXAMPLE OF SECTION 6.1

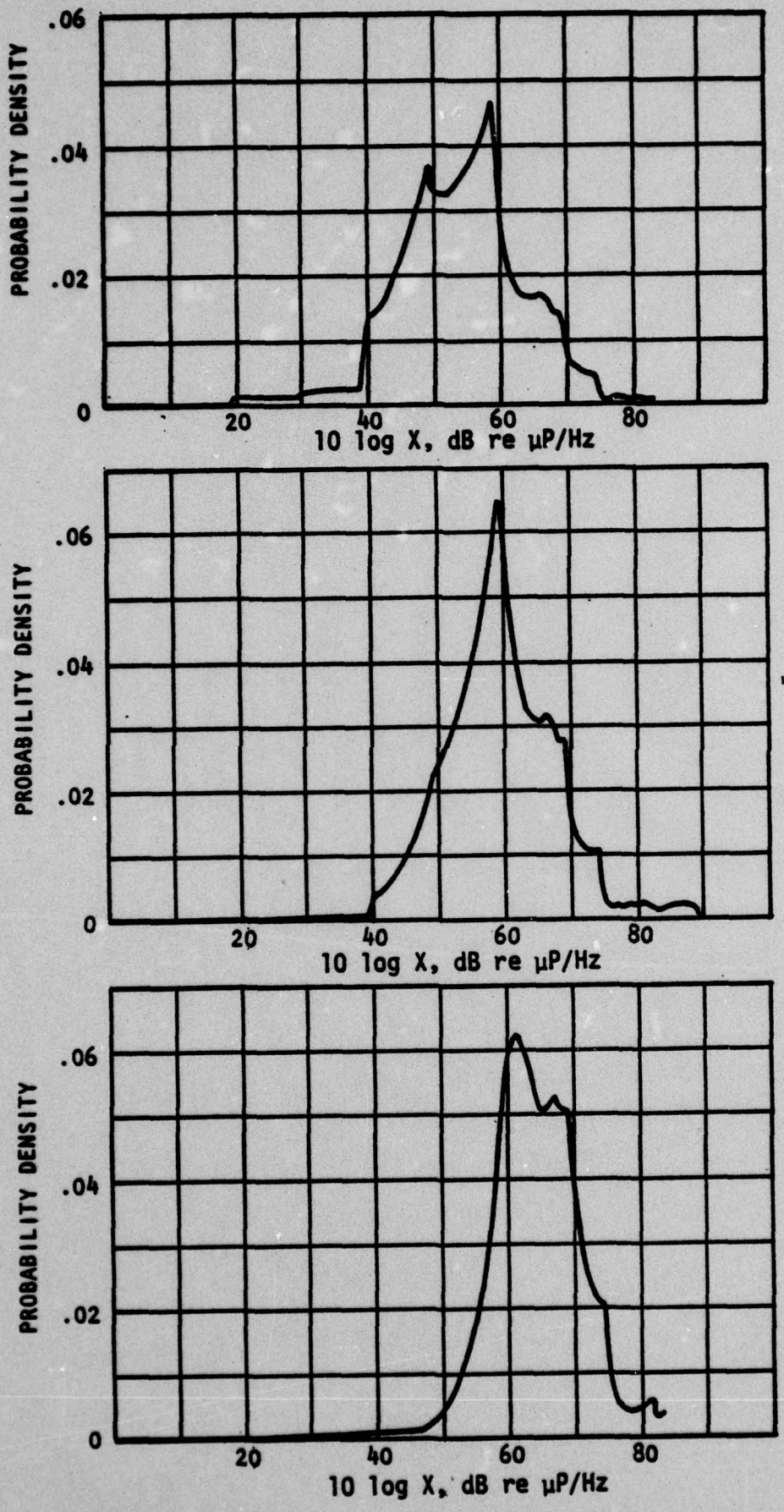

FIGURE 6.2 PROBABILITY DENSITY FUNCTIONS OF THE RECEIVED NOISE FOR THREE SHIP TRAFFIC DENSITIES:
(a) 0.025 ships/n.m. (b) 0.050 ships/n.m. (c) 0.100 ships/n.m.

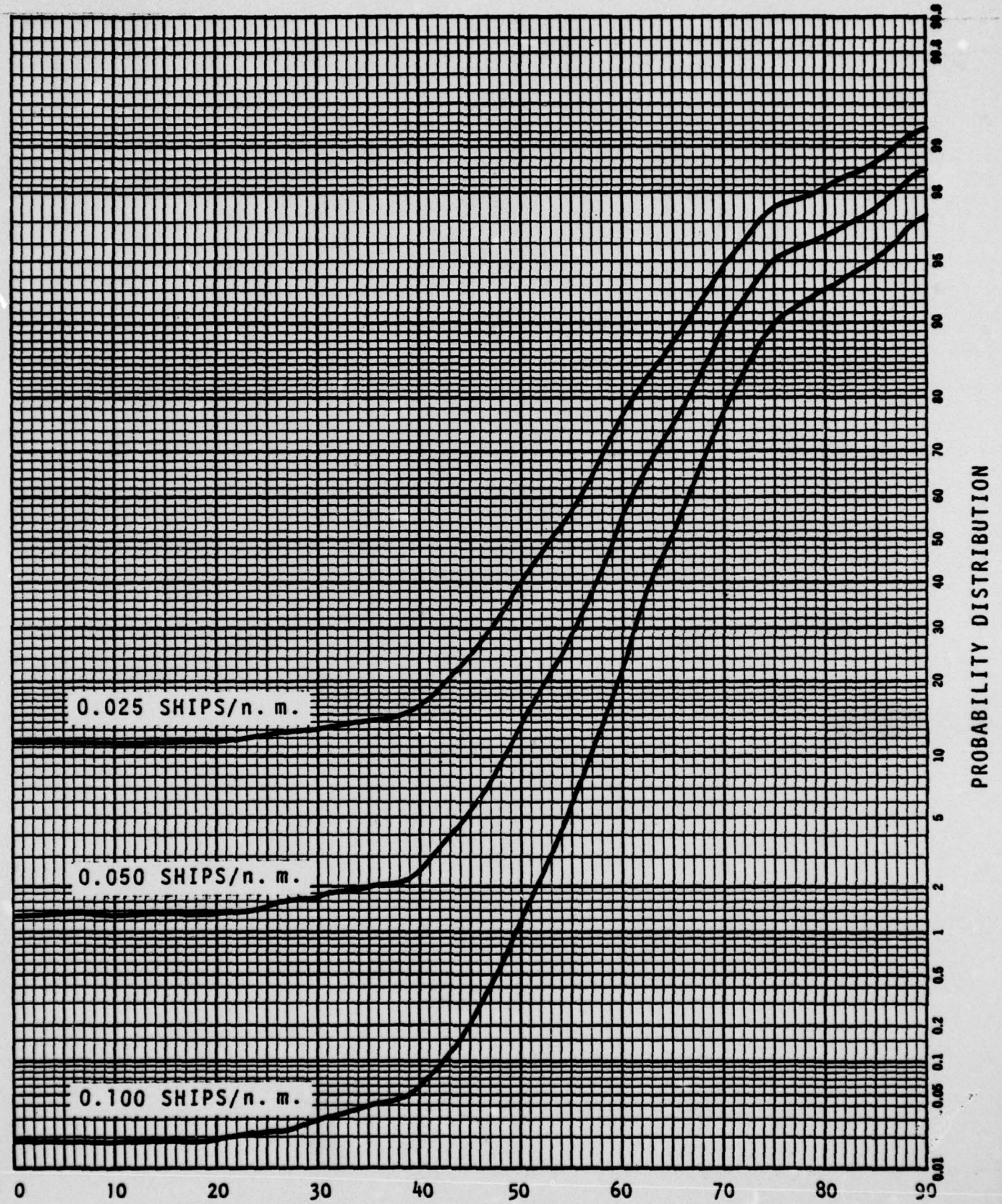

FIGURE 6.3 PROBABILITY DISTRIBUTION FUNCTIONS OF THE RECEIVED NOISE FOR THREE SHIP TRAFFIC DENSITIES

Table 6.1. Some Statistical Measures of the Recieved Noise for Three Ship Traffic Densities

Traffic Density		Average Number of Ships	Probability of No Noise	Mean M_X $(\mu P)^2$	Standard Deviation σ_X $(\mu P)^2$	σ_X / M_X
Large Ships (Ships/n.m.)	Small Ships (Ships/n.m.)					
0.025	0.025	2.136	0.118	1.762×10^6	7.259×10^6	4.120
0.050	0.050	4.272	0.014	3.449×10^6	1.001×10^7	2.902
0.100	0.100	8.544	0.0002	7.005×10^6	1.527×10^7	2.180

For the first case, the traffic density was 0.025 large merchant ships and 0.025 small merchant ships per nautical mile. In the second case the traffic density was double that of the first, while the third case was double that of the second. The average number of ships in the sector and the mean value of received noise (in power) increased by a factor of two from one case to the next, as expected. The probability of no noise goes from 11.8% for light shipping, down to 0.02% for the case of heavy shipping as expected. The ratio of the standard deviation to the mean is proportional to $\frac{1}{\sqrt{k}}$, where k = ships/n.m. This result agrees with expectations based on Campbell's Theorem.

The probability density functions as shown in Figure 6.2 exhibit two distinct peaks. This is what is expected since there are two types of sources. As the traffic density decreases, more detail can be seen in the probability density due to the detail in the source densities.

6.2 Example 2 — Variation in Range

For the second example, the ship traffic density was fixed at 0.05 large merchant ships and 0.05 small merchant ships per nautical mile. The sensor parameters were the same as in Section 6.1. The route parameters were the same as for the example of Section 6.1 except two different cases were processed with different ranges from the sensor to the center of the sector. In the first case, the range was 541.5 n.m. In the second case, it was reduced to 244.3 n.m. Figure 6.4 shows the route and sensor geometry for the two cases of this example, and gives the relevant parameters.

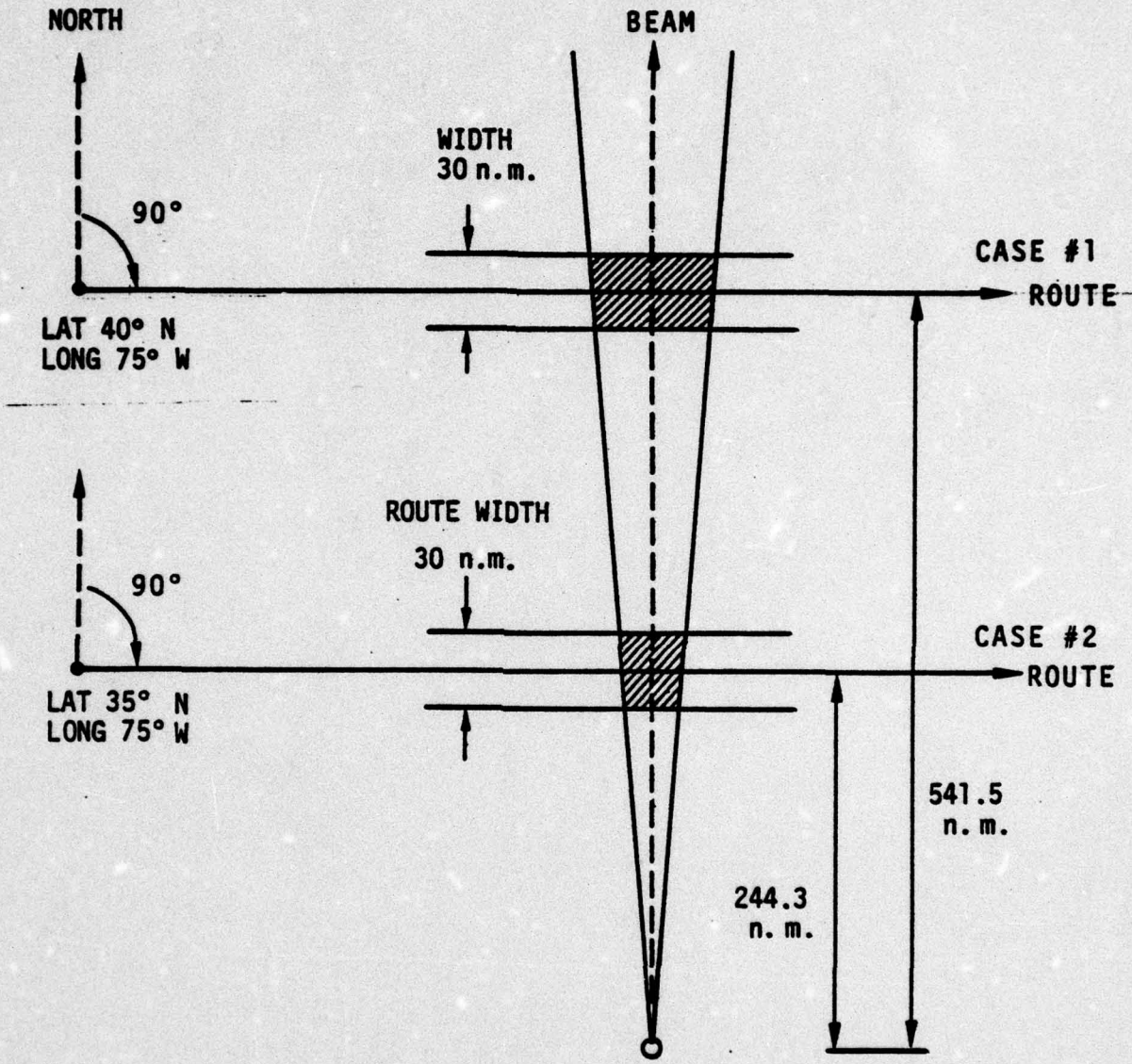

Beamwidth = 5°
Beam Bearing = 0°

LAT : 30° NORTH
LONG: 60° WEST
FREQ = 100 Hz

SHIP DENSITY:
0.05 large and 0.05 small per n. m.

FIGURE 6.4 ROUTE AND SENSOR GEOMETRY FOR THE EXAMPLE OF SECTION 6.2

Figure 6.5 shows the probability density functions of received noise for the two different ranges. Figure 6.6 shows the corresponding probability distribution functions. Statistical measures for the two cases are presented in Table 6.2.

When the range was decreased by a factor of 2.2, the mean increased less than 1% and the standard deviation increased by about 18%. This is due to the effect of the decrease in transmission loss at the closer range being offset by the decrease in the size of the sector and hence in the average number of ships. This effect is also apparent from the 1.4% probability of receiving no noise from the longer range as compared with the 14.4% probability of receiving no noise at the closer range. Again there are fewer ships in the sector at the closer range. These results are as expected.

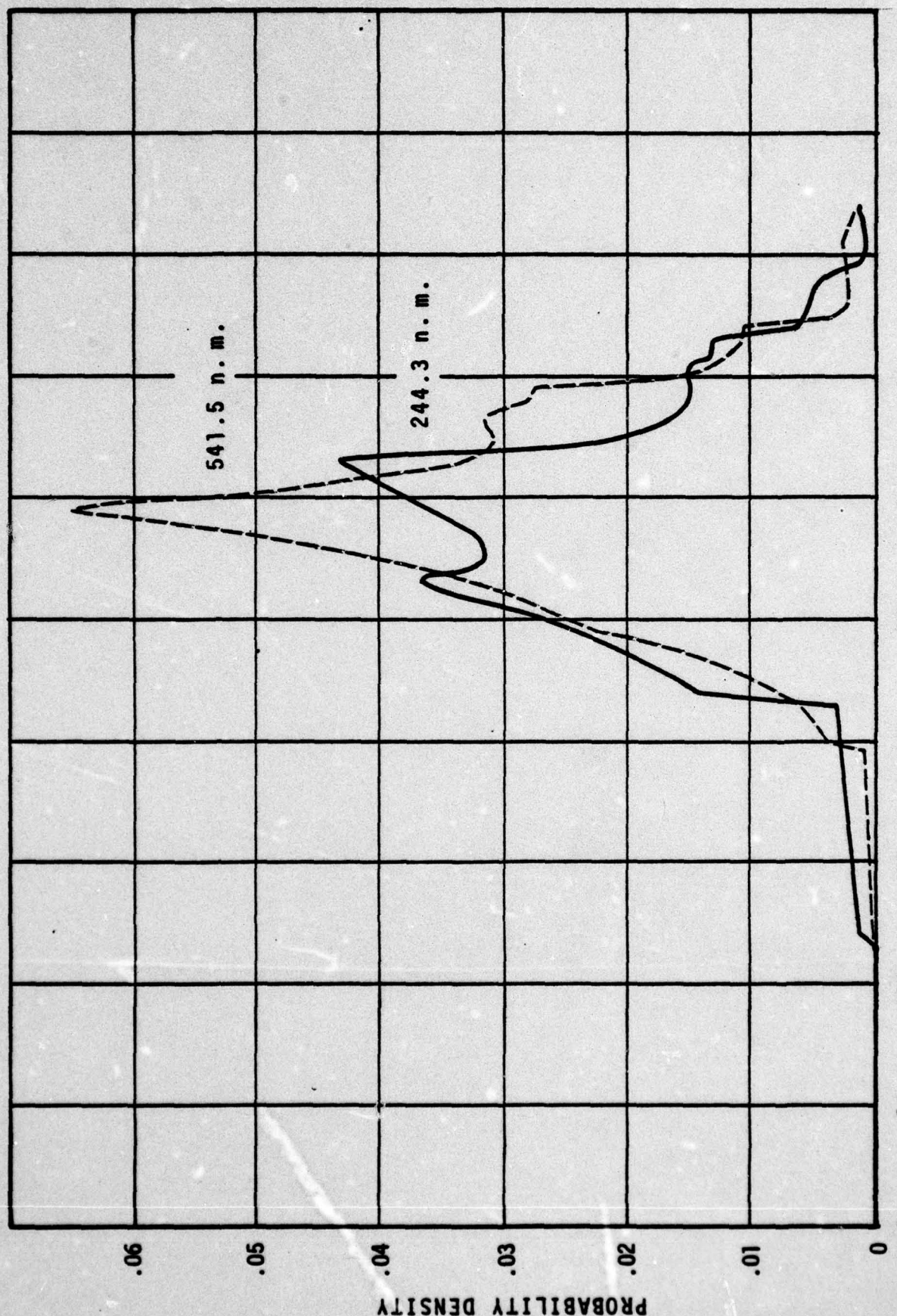

FIGURE 6.5 PROBABILITY DENSITY FUNCTIONS OF RECEIVED NOISE FOR TWO DIFFERENT RANGES

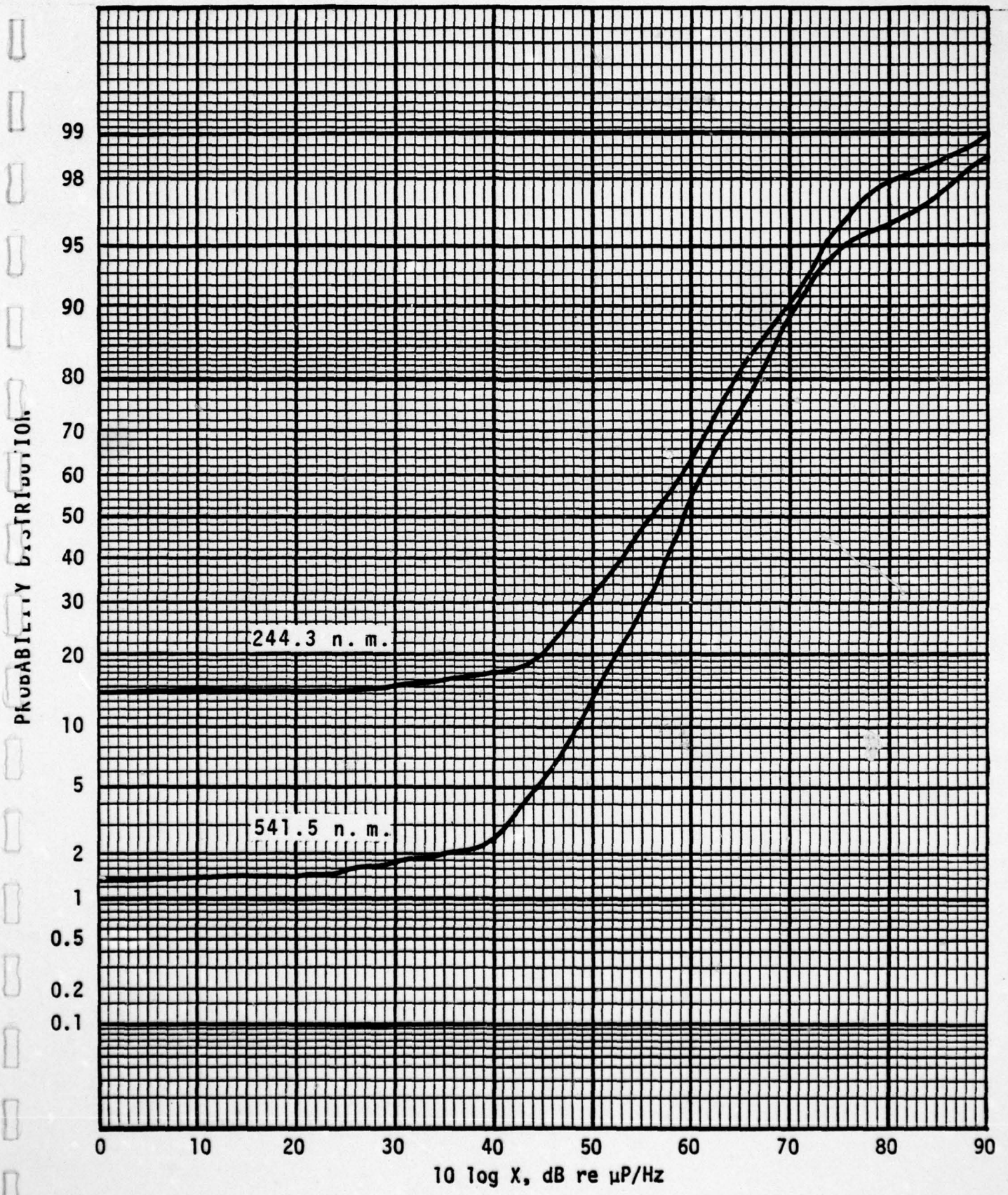

FIGURE 6.6 PROBABILITY DISTRIBUTION FUNCTIONS OF RECEIVED NOISE FOR TWO RANGES

AD-A046 714 BOLT BERANEK AND NEWMAN INC ARLINGTON VA F/G 20/1
STATISTICAL MEASURES OF AMBIENT NOISE: ALGORITHMS, PROGRAM, AND--ETC(U)
JUN 77 M MOLL, R M ZESKIND, F J SULLIVAN N00014-71-C-0303
UNCLASSIFIED BBN-3390 NL

2 OF 2
AD A046714

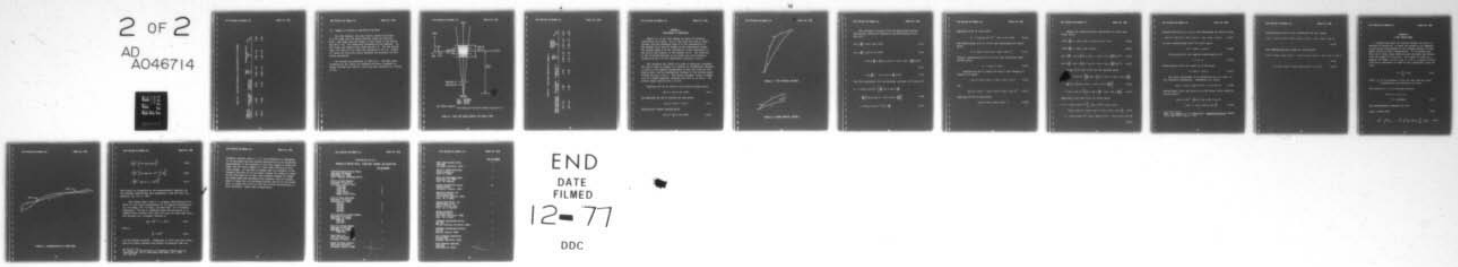

END
DATE FILMED
12-77
DDC

Table 6.2. Statistical Measures of Received Noise for Two Ranges

Range to Interaction (n.m.)	Average Number of Ships	Probability of No Noise	Mean $(\mu P)^2$ M_X	Standard Deviation $(\mu P)^2$ σ_X	σ_X / M_X
541.5	4.272	0.014	3.449×10^6	1.001×10^7	2.902
244.3	1.938	0.144	3.465×10^6	1.182×10^7	3.411

6.3 Example 3 — Variation in the Width of the Route

For this example, the ship traffic density was fixed at 0.05 large and 0.05 small merchant ships per nautical mile. The range from the sensor to the center of the sector was 244.3 n.m. Two cases were processed on the computer. In the first, the width of the route was 30 n.m. For the second case, the width of the route was increased to 60 n.m. Figure 6.7 shows the route and sensor geometry and presents the pertinent parameters.

The results are presented in Table 6.3. The mean value increased by 18%, while the standard deviation increased by almost 50% when the width of the route was increased by a factor of two.

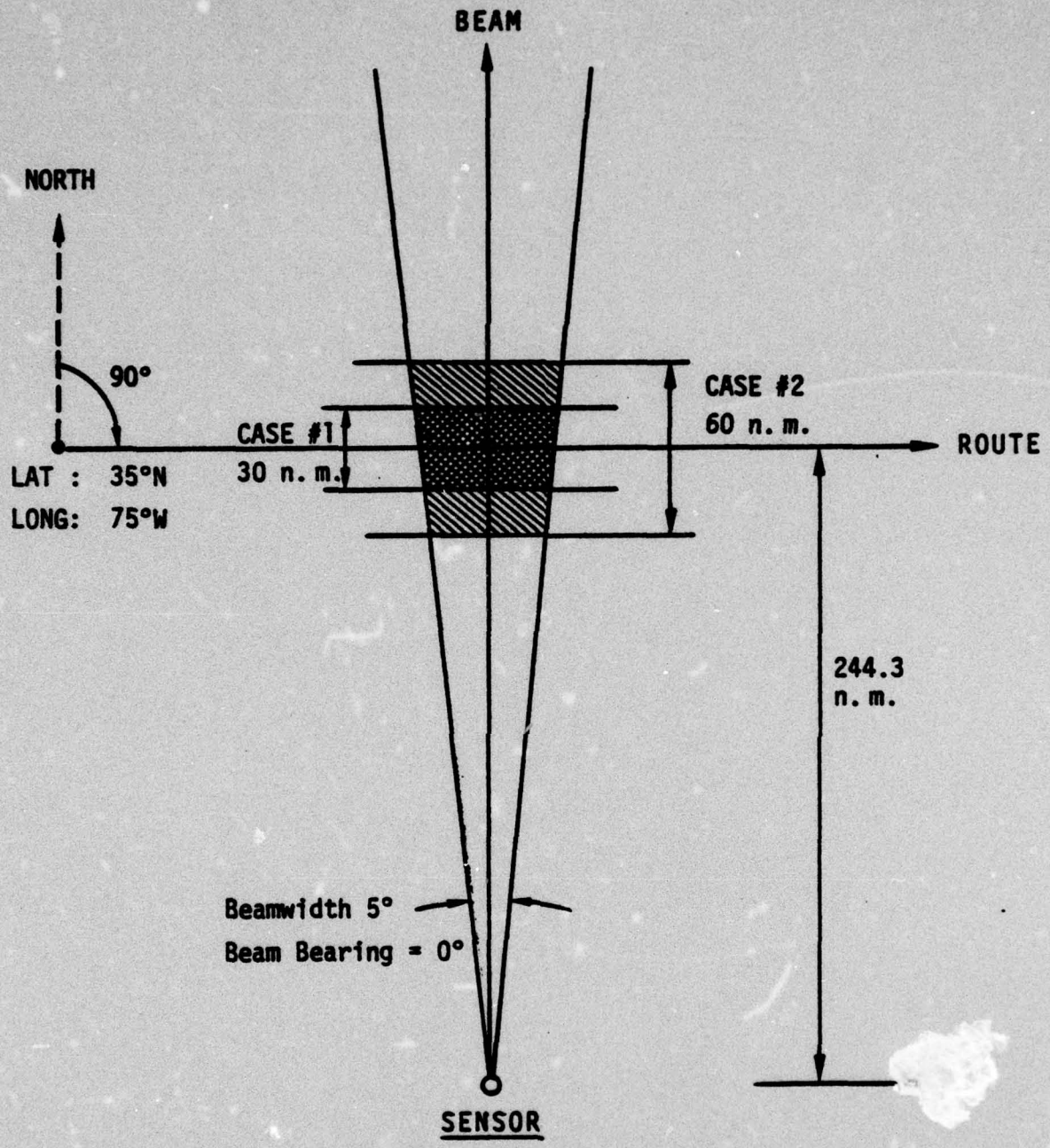

SHIP TRAFFIC DENSITY:

0.05 large and 0.05 small merchant ships per n.m.

FIGURE 6.7 ROUTE AND SENSOR GEOMETRY FOR EXAMPLE THREE

Table 6.3. Statistical Measures for Example 3

Route Uncertainty / Route Unvertainty	Average Number of Ships	Probability of No Noise	Mean $(\mu P)^2$ M_χ	Standard Deviation $(\mu P)^2$ σ_χ	σ_χ / M_χ
30.0 n.m.	1.938	0.144	3.465×10^6	1.182×10^7	3.411
60.0 n.m.	1.939	0.144	4.117×10^6	1.739×10^7	4.224

APPENDIX A
RELATIONSHIP OF COORDINATES

Figure 2.1 of the text showed two pairs of position coordinates for a ship. All of the lines are arcs of great circles, and the reference point R is the intersection of the nominal route and the center of the observation sector. The surface angle F is the orientation of the centerline of the sector with respect to the nominal route. The objective of the following analysis is to relate the route-oriented variables g and q to the observation variables r and D.

The variables are linked by a pair of spherical triangles. The first, shown in Figure A.1, defines an intermediate variable d, which is the angular displacement of the ship from the reference point, and an intermediate variable R, the surface angle between the arcs d and s. The second triangle, shown in Figure A.2, is a right spherical triangle with arcs d, g, and q. The surface angle opposite arc q is R-F.

Applying the law of sines to the second triangle gives

$$\sin q = \sin d \sin (R-F) \qquad \text{(A-1)}$$

and applying the law of cosines for arcs gives

$$\cos g = \cos d \div \cos q \qquad \text{(A-2)}$$

Applying yet another theorem gives

$$\sin g = \tan q \cot (R-F) \qquad \text{(A-3)}$$

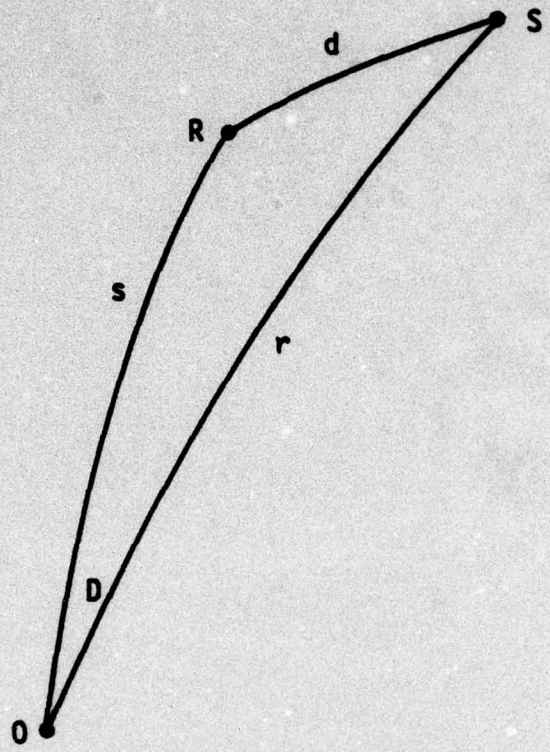

FIGURE A.1 FIRST SPHERICAL TRIANGLE

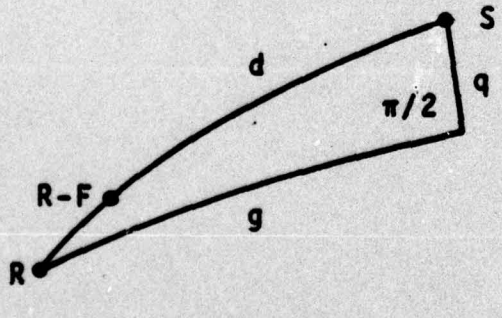

FIGURE A.2 SECOND SPHERICAL TRIANGLE

The Jacobian is derived from the appropriate partial derivatives, which are obtained by differentiating (A-1) and (A-2)

$$\cos q \frac{\partial q}{\partial d} = \cos d \sin (R-F) \tag{A-4}$$

$$\cos q \frac{\partial q}{\partial R} = \sin d \cos (R-F) \tag{A-5}$$

$$- \sin g \frac{\partial g}{\partial d} = \left(-\cos q \sin d + \cos d \sin q \frac{\partial q}{\partial d}\right) \cos^{-2} q \tag{A-6}$$

$$- \sin \frac{\partial g}{\partial R} = \cos d \sin q \frac{\partial q}{\partial R} \cos^{-2} q \tag{A-7}$$

The first expression for the Jacobian utilizes (A-6) and (A-7)

$$J_1 = -(\sin g \cos^2 q)^{-1} \left[\frac{\partial q}{\partial d} \cos d \sin q \frac{\partial q}{\partial R} - \frac{\partial q}{\partial R}\left(-\cos g \sin d + \cos d \sin q \frac{\partial q}{\partial d}\right)\right] \tag{A-8}$$

$$= -(\sin g \cos q)^{-1} \sin d \frac{\partial q}{\partial R} \tag{A-9}$$

Employing (A-5) in (A-9) gives

$$J_1 = -(\sin g \cos^2 q)^{-1} \sin^2 d \cos (R-F) \qquad \text{(A-10)}$$

and substituting (A-3) in (A-10) and simplifying the result gives

$$J_1 = -\sin^2 d \sin (R-F) (\sin q \cos q)^{-1} \qquad \text{(A-11)}$$

Finally, substituting (A-1) in (A-11) and cancelling common factors gives

$$J_1 = -\sin d \div \cos q \qquad \text{(A-12)}$$

Applying the law of cosins for arcs to the triangle in Figure (A.1) gives

$$\cos d = \cos s \cos r + \sin s \sin r \cos D \qquad \text{(A-13)}$$

and

$$\cos R = (\cos r - \cos s \cos d) (\sin s \sin d)^{-1} \qquad \text{(A-14)}$$

Applying the law of sins gives

$$\sin R = \sin r \sin D \sin^{-1} d \qquad \text{(A-15)}$$

Taking the required partial derivatives of (A-13) and (A-15) gives

$$-\sin d \frac{\partial d}{\partial r} = -\cos s \sin r + \sin s \cos r \cos D \quad \text{(A-16)}$$

$$-\sin d \frac{\partial d}{\partial D} = -\sin s \sin r \sin D \quad \text{(A-17)}$$

$$\cos R \frac{\partial R}{\partial r} = \sin D \left(\sin d \cos r - \sin r \cos d \frac{\partial d}{\partial r}\right) \sin^{-2} d \quad \text{(A-18)}$$

$$\cos R \frac{\partial R}{\partial D} = \sin r \left(\sin d \cos D - \sin r \cos d \frac{\partial d}{\partial D}\right) \sin^{-2} d \quad \text{(A-19)}$$

Using (A-18) and (A-19) for the Jacobian gives

$$(\cos R \sin^2 d)^{-1} \left[\frac{\partial d}{\partial r} \sin r \left(\sin d \cos D - \sin r \cos d \frac{\partial d}{\partial D}\right)\right.$$

$$\left. - \frac{\partial d}{\partial D} \sin D \left(\sin d \cos r - \sin r \cos d \frac{\partial d}{\partial D}\right)\right] \quad \text{(A-20)}$$

$$= (\cos R \sin d)^{-1} \left[\sin r \cos D \frac{\partial d}{\partial r} - \cos r \sin D \frac{\partial d}{\partial D}\right] \quad \text{(A-21)}$$

Employing (A-16) and (A-17) in (A-21) gives

$$J_2 = -(\cos R \sin^2 d)^{-1} \left[\cos r \sin^2 D \sin s \sin r\right.$$

$$\left. + \sin r \cos D (-\cos s \sin r + \sin s \cos r \cos D)\right] \quad \text{(A-22)}$$

$$= -(\cos R \sin^2 d)^{-1} \sin r [\sin s \cos r - \cos s \sin r \cos D] \quad \text{(A-23)}$$

Substituting (A-13) in (A-14) and simplifying the result yields

$$\cos R = (\sin d)^{-1} (\sin s \cos r - \cos s \sin r \cos D) \quad \text{(A-24)}$$

In turn, substituting (A-24) in (A-23) gives

$$J_2 = - \sin r \div \sin d \quad \text{(A-25)}$$

The Jacobian for the complete transformation is*

$$J = J_1 J_2 \quad \text{(A-26)}$$

Substituting (A-12) and (A-25) in (A-26) gives

$$J = \sin r \div \cos q \quad \text{(A-27)}$$

The final requirement is an expression for q in terms of the observation parameters. Expanding (A-1) gives

$$\sin q = \sin d (\sin R \cos F - \cos R \sin F) \quad \text{(A-28)}$$

Substituting (A-14) and (A-15) in (A-28) gives, after simplifying the result

$$\sin q = \sin^{-1} s \left[\sin r \sin s \sin D \cos F - (\cos r - \cos s \cos d) \sin F\right] \quad \text{(A-29)}$$

*See, for example, I. S. Solkolnikov, Advanced Calculus, McGraw Hill, New York, 1939, p. 438.

Substituting (A-13) in the coefficient for sin F gives

$$\cos r - \cos s \cos d = \sin s (\sin s \cos r - \cos s \sin r \cos D), \quad \text{(A-30)}$$

and substituting this result in (A-29) gives

$$\sin q = \sin r \sin D \cos F + (\cos s \sin r \cos D - \sin s \cos r) \sin F \quad \text{(A-31)}$$

$$\approx D \sin r \cos F + \sin (r-s) \sin F, \; D \leq \pi/18 \quad \text{(A-32)}$$

APPENDIX B
A SHIP TRAFFIC MODEL

A single-loop model for traffic between two ports is depicted in Figure B.1 in which the length of the segments s_A and s_B are proportional to the average fraction of time spent in ports A and B respectively. It is assumed that there are n ships whose positions are uniformly distributed over the length ℓ of the loop. The number of ships on a segment of length s of the loop ($s < \ell$) is a random variable that can be expressed in terms of the coordinates along the loop:

$$N = \sum_{i=1}^{n} c(X_i) \qquad \text{(B-1)}$$

where X_i is the distance of the ith ship from the point 0 measured in the direction of travel.

The function c( ) is a counting function:

$$c(x) = 1, \quad 0 \leq x \leq s$$

$$= 0, \quad \text{elsewhere} \qquad \text{(B-2)}$$

The characteristic function for N is

$$\Phi_N(\omega) = E[\exp j\omega N] \qquad \text{(B-3)}$$

$$= \ell^{-1} \int_0^{\ell} dx, \ldots\ldots \ell^{-1} \int_0^{\ell} dx_n \exp j\omega \sum_{i=1}^{n} c(x_i) \qquad \text{(B-4)}$$

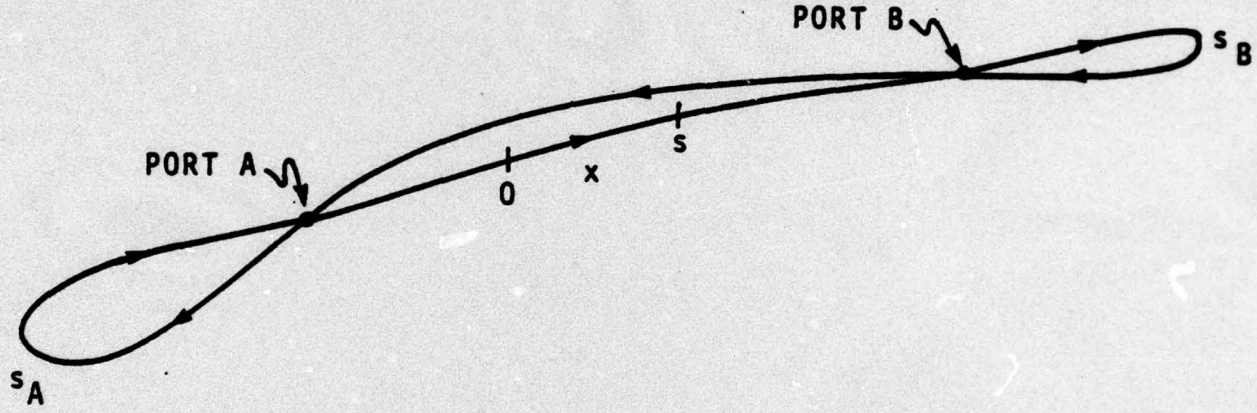

FIGURE B.1 REPRESENTATION OF A TRADE ROUTE

$$= \left[\ell^{-1} \int_0^{\ell} dx \exp j\omega c(x)\right]^n \qquad \text{(B-5)}$$

$$= \left[\ell^{-1} \int_0^{s} dx \exp j\omega + \ell^{-1} \int_s^{\ell} dx\right]^n \qquad \text{(B-6)}$$

$$= \left[s\ell^{-1} \exp j\omega + 1 - s\ell^{-1}\right]^n \qquad \text{(B-7)}$$

This result is recognized as the characteristic function for the binomial distribution with parameters n and $s\ell^{-1}$ (see e.g., Papoulis, op. cit, p. 154).

This simple model leads to a binomial distribution for n, which in turn can be approximated by the Poisson distribution if n is large, $s\ell^{-1}$ is small, and when $ns\ell^{-1}$ is of moderate magnitude.* One way of comparing these distributions is to compare their variance when they both have the same mean value. The variance for a binomial variable is

$$\sigma_B^2 = ns\ell^{-1} (1 - s\ell^{-1}) \qquad \text{(B-8)}$$

and is

$$\sigma_P^2 = ns\ell^{-1} \qquad \text{(B-9)}$$

for the Poisson variable. Comparison of (B-8) and (B-9) shows that the Poisson variable has greater fluctuation than the

*W. Feller, An Introduction to Probability Theory and its Applications, Vol I, John Wiley and Sons, Inc., 1957, pp. 142-143.

binomial; however, when $s << l$, the difference is negligable. It is concluded that the Poisson distribution is an acceptable approximation to the binomial if the total number of ships are high, and the route segment is a very small fraction of the route length. It can also be argued that the variance of the binomial distribution is too small because the number of ships on the loop does not in fact stay constant because (1) ships are being added and withdrawn from commerce, and (2) certain types of ships will be switching between various of the routes. Thus, it might well turn out that the Poisson distribution is more preferable under some circumstances.

Distribution List for

MEASURES OF AMBIENT NOISE: ALGORITHMS, PROGRAM, AND PREDICTIONS

	No. of Copies
Advanced Research Project Agency Department of Defense Washington, DC 20350 Attn: Tactical Technology Office	1
Office of Naval Research Department of the Navy Arlington, Virginia 22217	
(Code 220)	1
(Code 436)	1
(Code 431)	2
(Code 102-OS)	1
NORDA Liaison Office	1
Chief of Naval Operations Department of the Navy Washington, DC 20350	
(Op-987)	1
(Op-951)	1
(Op-955)	1
(Op-961)	1
(Op-966)	1
Naval Electronic Systems Command Department of the Navy Washington, DC 20360	
(PME-124)	1
ELEX 320	1
Naval Air Systems Command Department of the Navy Washington, DC 20360	
(Code 370)	1
Tetra Tech, Inc. 1901 Fort Myer Drive Arlington, Virginia 22209	1
Center for Naval Analysis 1401 Wilson Boulevard Arlington, Virginia 22209	1

	No. of copies
Naval Ocean Systems Center Code 8000 San Diego, California 92152	1
Daniel H. Wagner Associates Station Square One Paoli, PA 19301	1
Naval Air Development Center Warminster, PA 18974 Attn: Mr. Metersky	1
Defense Documentation Center Cameron Station Alexandria, Virginia 22313	12
Operations Research Inc. 1400 Spring Street Silver Spring, Maryland 20910 Attn: Dr. E. Moses	1
Science Applications, Inc. 8400 Westpark Drive McLean, Virginia 22101 Attn: Dr. C. Spofford	1
Xybion Corporation 65 Madison Avenue Morristown, New Jersey 07960 Attn: Dr. H. Hurd	1
Commander Oceansystems Pacific Box 1390 FPO San Francisco, California 96610	1
Commander Oceansystems Atlantic Box 100 Norfolk, Virginia 23511	1
Bell Telephone Laboratories Whippany Road Whippany, New Jersey 07981	1
Naval Research Laboratory Code 8109 Washington, DC 20375	1